Multiple Binding Sites on the Pyrin Domain of ASC Protein Allow Self-association and Interaction with NLRP3 Protein*[S]

Parimala R. Vajjhala[‡], Ruth E. Mirams[‡], and Justine M. Hill[‡§1]

From the ‡School of Chemistry and Molecular Biosciences and §Centre for Advanced Imaging, The University of Queensland, Brisbane, Queensland 4072, Australia

Background: Pyrin domains (PYDs) mediate the assembly of inflammasome complexes, but PYD interaction modes are not well characterized.
Results: Interaction sites were identified on the PYD of the inflammasome adaptor protein, ASC.
Conclusion: ASC PYD has multiple binding sites allowing self-association and interaction with binding partners.
Significance: Understanding molecular details of inflammasome assembly may lead to development of anti-inflammatory agents.

A key process underlying an innate immune response to pathogens or cellular stress is activation of members of the NOD-like receptor family, such as NLRP3, to assemble caspase-1-activating inflammasome complexes. Activated caspase-1 processes proinflammatory cytokines into active forms that mediate inflammation. Activation of the NLRP3 inflammasome is also associated with common diseases including cardiovascular disease, diabetes, chronic kidney disease, and Alzheimer disease. However, the molecular details of NLRP3 inflammasome assembly are not established. The adaptor protein ASC plays a key role in inflammasome assembly. It is composed of an N-terminal pyrin domain (PYD) and a C-terminal caspase recruitment domain, which are protein interaction domains of the death fold superfamily. ASC interacts with NLRP3 via a homotypic PYD interaction and recruits procaspase-1 via a homotypic caspase recruitment domain interaction. Here we demonstrate that ASC PYD contains two distinct binding sites important for self-association and interaction with NLRP3 and the modulatory protein POP1. Modeling of the homodimeric ASC PYD complex formed via an asymmetric interaction using both sites resembles a type I interaction found in other death fold domain complexes. This interaction mode also permits assembly of ASC PYDs into filaments. Furthermore, a type I binding mode is likely conserved in interactions with NLRP3 and POP1, because residues critical for interaction of ASC PYD are conserved in these PYDs. We also demonstrate that ASC PYD can simultaneously self-associate and interact with NLRP3, rationalizing the model whereby ASC self-association upon recruitment to NLRP3 promotes clustering and activation of procaspase-1.

Activation of the innate immune response to pathogens and various cellular stress signals is mediated by pattern recognition receptors that include members of the NOD-like receptor (NLR)[2] family. NLRs are characterized by the presence of a central nucleotide-binding domain and a C-terminal leucine-rich repeat domain (1–4). Upon activation, certain NLRs including NLRC4, NLRP1, NLRP3, and NLRP7 assemble into caspase-1-activating complexes termed inflammasomes (5–9). Inflammasomes mediate proximity-induced autoactivation of caspase-1, which subsequently cleaves prointerleukin-1β and prointerleukin-18 into their active forms to mediate an inflammatory response (10–12). Uncontrolled inflammasome activity caused by gain of function mutations in NLRP3 can cause severe damage to the body as observed in autoinflammatory syndromes such as Muckle-Wells syndrome, familial cold autoinflammatory syndrome, and neonatal onset multisystem inflammatory disease (13). The NLRP3 inflammasome has been particularly well studied because it is activated in response to a wide range of danger and stress signals (14–21) and has been implicated in the progression of a number of common diseases such as cardiovascular disease, type 2 diabetes, chronic kidney disease, Alzheimer disease, and gout (15, 22–25). Consequently, the NLRP3 inflammasome is a potential target for therapeutic treatment of a wide range of diseases (26, 27). However, despite intensive research on the inflammasome, the molecular details of its assembly and regulation remain to be elucidated.

Inflammasome assembly is mediated by protein interaction domains belonging to the death fold superfamily. This large superfamily is comprised of the death domain (DD), death effector domain, caspase recruitment domain (CARD), and pyrin domain (PYD) subfamilies (28, 29). These domains typically exhibit a characteristic six-helix bundle fold and mediate homotypic interactions between domains of the same subfamily. The NLRP subfamily of NLRs, such as NLRP1, NLRP3, and NLRP7, contain an N-terminal PYD and upon activation are proposed to oligomerize via their nucleotide binding domain and recruit the adaptor protein ASC (apoptosis-associated speck-like protein containing a CARD) (6, 7, 9, 12). ASC is

---

[S] This article contains supplemental Figs. S1–S8.
[1] To whom correspondence should be addressed: School of Chemistry and Molecular Biosciences, The University of Queensland, Brisbane QLD 4072, Australia. Tel.: 61-7-3365-3925; Fax: 61-7-3365-4273; E-mail: justine. hill1@gmail.com.

[2] The abbreviations used are: NLR, NOD-like receptor; CARD, caspase recruitment domain; DD, death domain; PYD, pyrin domain.

comprised of an N-terminal PYD and a C-terminal CARD and plays a critical role in the assembly of NLRP inflammasomes (6, 7, 30). ASC is recruited to the NLRP oligomer via a homotypic PYD interaction, whereas a homotypic CARD interaction between ASC and procaspase-1 recruits the latter to the inflammasome.

Intriguingly, ASC has been suggested to self-associate via both its PYD and CARD domains (31, 32). However, it is not clear whether ASC self-associates upon recruitment to the inflammasome because its PYD and CARD domains are engaged in interactions with NLRP3 and procaspase-1, respectively. Furthermore, it is unclear how PYD-containing proteins such as POP1 and Pyrin (33, 34) modulate ASC function in inflammasome assembly. Apart from its role in inflammasome assembly, ASC assembles into a speck-like structure upon stimulation with apoptotic or inflammatory stimuli (35, 36). High magnification microscopy indicates that the specks are filamentous aggregates (32). The ASC specks induced by inflammatory stimuli, termed pyroptosomes, can induce caspase-1 activation and mediate pyroptotic cell death (36). However, the molecular arrangement of ASC in the pyroptosome is not known.

At present, the molecular basis of PYD and CARD interactions that mediate inflammasome assembly are not known. In particular, there is no structure for a PYD complex available. The structures of various PYDs in isolation have been determined, including ASC (37), NLRP1 (38), NLRP3 (39), NLRP7 (40), NLRP12 (41), POP1 (42), and murine NLRP10 (Protein Data Bank ID code 2DO9). Several PYDs including ASC, POP1, and NLRP3 have distinct positively and negatively charged surface patches, and this has led to the proposal that electrostatic interactions will be critical for PYD interactions (37, 39, 42). However, the interaction sites have not been systematically mapped for any PYDs. In this study, we used a site-directed mutagenesis approach to investigate the molecular interactions of ASC PYD important for self-association, NLRP3 inflammasome assembly, and interaction with the modulatory protein POP1. Structural integrity of mutants with reduced binding was confirmed using NMR spectroscopy to demonstrate a direct role for these residues in interaction. Using the information obtained from our mutagenesis data, we generated a model of the ASC PYD homodimer that illustrates the binding mode of PYDs. We also investigated whether self-association of the ASC PYD and interaction with NLRP3 are mutual or exclusive events. Finally, we examined the effect of POP1 on ASC interaction with NLRP3. Together, our data provide new insights into the binding mode of PYDs and assembly of the pyroptosome and NLRP3 inflammasome complexes.

EXPERIMENTAL PROCEDURES

Plasmids—For expression in *Escherichia coli* with an N-terminal GST tag, the cDNA fragment encoding ASC PYD (residues 1–91) was subcloned into pGEX-4T-1 (GE Healthcare). For expression in *E. coli* with an N-terminal His$_6$ tag, the cDNA fragment encoding residues 1–96 of ASC was subcloned into pQE-30 (Qiagen). Specific point mutations were introduced into ASC PYD using the QuikChange site-directed mutagenesis approach (Stratagene). Full-length POP1 (residues 1–89) was

subcloned into pET-21a (Novagen) for *in vitro* translation, and His$_6$-tagged POP1 was expressed in *E. coli* as previously described (42). The Pyrin PYD (residues 1–92) was subcloned into pET-28b (Novagen) for expression with a C-terminal His$_6$ tag. Full-length ASC (residues 1–195) was expressed in mammalian cells using pcDNA3-ASC. Full-length NLRP3 was expressed in mammalian cells with an N-terminal His$_6$ tag and a C-terminal FLAG tag using pcDNA3.1/His B plasmid. For expression in mammalian cells, full-length ASC, ASC PYD, and POP1 were amplified with an N-terminal Myc tag and subcloned into pcDNA3.1(+) (Invitrogen). Sequences of all constructs were verified by automated DNA sequencing (Australian Genome Research Facility).

Protein Expression and Purification—His$_6$-tagged proteins were expressed in *E. coli* BL21 cells (pQE-30 plasmid) or BL21(DE3) cells (pET plasmids). To express wild-type and mutant ASC PYDs, the cells were grown at 37 °C to an optical density ($A_{600\text{ nm}}$) of 0.4 and then induced with 1 mM isopropyl β-D-thiogalactopyranoside at 20 °C overnight. To express POP1 and the Pyrin PYD, cells were grown at 37 °C to an optical density of 1.0 and then induced with 1 mM isopropyl β-D-thiogalactopyranoside at 37 °C for 5 h. Uniformly ^{15}N- and ^{13}C/^{15}N-labeled proteins for NMR studies were expressed in minimal medium containing ^{15}NH$_4$Cl (1 g/liter) and [^{13}C]glucose (2 g/liter) as the sole nitrogen and carbon sources, as previously described (43). His$_6$-tagged proteins were purified using Ni^{2+} affinity followed by size exclusion chromatography on a Sephacryl S-100 HR column (GE Healthcare). GST-ASC PYD (wild-type and mutant) fusion proteins were expressed in *E. coli* BL21 cells and batch-purified using glutathione-agarose beads (Sigma).

In Vitro Protein Interaction Assays—NLRP3, ASC, POP1, and Pyrin PYD were expressed *in vitro* using the TNT T7 coupled reticulocyte lysate system (Promega) in the presence of [^{35}S]methionine (PerkinElmer Life Sciences). The ^{35}S-labeled proteins were incubated with GST-tagged wild-type or mutant ASC PYD bound to glutathione-agarose in 150 µl of binding buffer (50 mM HEPES pH 7.4, 50 mM NaCl, 5 mM EDTA, 0.1% Nonidet P-40, 10% glycerol). The samples were incubated for 2 h at 4 °C and washed three times with 0.5 ml of binding buffer. Bound protein was eluted with SDS-PAGE sample buffer and separated by SDS-PAGE. ^{35}S-Labeled protein was detected by phosphorimaging. For competition binding studies, purified recombinant His$_6$-tagged POP1, ASC PYD, or Pyrin PYD was added to the binding reactions.

Co-immunoprecipitation Assays—HEK 293T cells were maintained in DMEM/F-12 medium supplemented with 10% fetal bovine serum. The cells were seeded in 6-well plates and transfected using FuGENE (Promega). After incubation for 24 h, the transfected cells were lysed by syringing in a hypotonic lysis buffer (20 mM HEPES pH 7.4, 10 mM KCl, 1 mM EDTA, 0.1 mM PMSF, 2 mg/ml leupeptin, 1 mM Na$_3$VO$_4$, 5 mM NaF). The cell lysate was centrifuged at 10,000 × g for 15 min at 4 °C, and the supernatant was diluted 1:1 with 2× immunoprecipitation buffer (100 mM Tris pH 7.8, 300 mM NaCl, 0.2% Nonidet P-40, 10 mM EDTA) and then filtered through a low protein binding Millex-GP 0.22-µm membrane (Millipore). The resulting soluble cell lysate was precleared using protein A Dynabeads (Invit-

rogen). The precleared cell lysate was incubated with 1 μl of anti-Myc antibody (clone 9B11; Cell Signaling Technology) or 5 μl of anti-FLAG antibody (DYKDDDDK tag antibody; Cell Signaling Technology) at 4 °C overnight. Protein A Dynabeads were added to each sample, incubated for 2 h, and then washed three times with immunoprecipitation buffer (50 mM Tris pH 7.8, 150 mM NaCl, 0.1% Nonidet P-40, 5 mM EDTA). Bead-bound proteins were eluted with SDS-PAGE sample buffer. Eluted proteins and cell lysates were separated by SDS-PAGE and immunoblotted using antibodies to ASC (Enzo Life Sciences), Myc tag (Cell Signaling Technology), FLAG tag (Cell Signaling Technology), and β-actin (Sigma-Aldrich) and developed using enhanced chemiluminescence.

NMR Spectroscopy—Samples for NMR contained 0.3–0.9 mM protein in 50 mM sodium phosphate pH 4.0, and 150 mM NaCl. NMR spectra were acquired at 25 °C on a Bruker Avance 750 MHz spectrometer equipped with a *z*-shielded gradient triple resonance probe. NMR spectra were processed with NMRPipe (44) and analyzed using CcpNmr (45). Two-dimensional ^1H-^{15}N HSQC spectra were recorded for wild-type ASC PYD and point mutants that affected interactions of the ASC PYD (R3A, D10A, E13A, K21A, R38A, R41A, D48A, D51A, and D54A). Backbone resonance assignments of wild-type ASC PYD were accomplished using 3D HNCO, HN(CA)CO, CBCA-(CO)NH, HNCACB, and C(CO)NH experiments (46). Mutation-induced chemical shift changes were calculated using weighted average values, $\Delta\delta_{av}$, with $\Delta\delta_{av} = \{[\Delta\delta(^1H^N)^2 + (0.2\Delta\delta(^{15}N))^2]/2\}^{1/2}$ (47). Assignments for the ^1H, ^{13}C, and ^{15}N backbone resonances of ASC PYD have been deposited in the BioMagResBank database with the accession number 18608.

HADDOCK Modeling—Modeling the ASC PYD homodimer structure was performed using the HADDOCK (High Ambiguity Driven protein-protein DOCKing) web server (48). The ASC PYD structure (Protein Data Bank ID code 1UCP) (37) was used as the starting structure for docking calculations. Active residues were defined based on mutagenesis data from this study and surface accessibility (>27% exposed to solvent). Residues Lys-21 and Arg-41 were defined as active residues for one ASC PYD molecule, whereas residues Glu-13, Asp-48, and Asp-51 were designated active residues for the second molecule. Passive residues were defined automatically. A total of 1000 complex structures were calculated using rigid body docking, with the best 200 structures subjected to further refinement and cluster analysis. The lowest energy cluster was chosen to represent the structure of the ASC PYD homodimer. Coordinates of the ASC PYD homodimer structure have been deposited in the Protein Model Data Base with the identification number PM0078339.

RESULTS

Overlapping Binding Sites on the ASC PYD Mediate Self-association and Interaction with NLRP3 and POP1—Because the ASC PYD mediates self-association, as well as ASC recruitment to NLRP3 and interaction with the modulatory protein POP1, we were interested to understand the binding mode for each of these different interactions. Although previous studies have suggested that highly charged surface patches are important for ASC PYD interactions (31, 37, 49), we used an unbiased

approach to design 16 alanine point mutations that span the surface of the ASC PYD to explore all potential modes of interaction. Only surface-exposed residues with a solvent accessibility greater than 27% were selected for mutagenesis to minimize any structural perturbations, and approximately two residues per helix were mutated to cover the entire surface (Fig. 1*A*). To assess the effect of mutations on the different interactions, wild-type and mutant ASC PYDs were expressed as GST fusion proteins and used in binding assays with *in vitro* translated ASC, NLRP3, or POP1. Interestingly, four point mutations (K21A, R41A, D48A, and D51A) abolished all interactions with ASC, whereas a fifth mutation (E13A) markedly reduced all interactions (Fig. 1, *B–D*). In addition, five other mutations (R3A, D10A, R38A, D54A, and Q84A) also diminished interaction with POP1 (Fig. 1*D*) but did not disrupt ASC self-association or NLRP3 binding.

To verify the importance of the five key residues (Glu-13, Lys-21, Arg-41, Asp-48, and Asp-51) for ASC PYD interactions, we tested the effect of mutating these residues on interactions of full-length ASC in a more physiologically relevant context. Co-expression of NLRP3, ASC, and procaspase-1 in HEK 293T cells has been shown to reconstitute a functionally active inflammasome (7), although HEK 293T cells normally do not express inflammasome components. Thus we used this cell line to study ASC interactions. Wild-type or mutant full-length ASC was co-expressed in HEK 293T cells with either FLAG-tagged NLRP3, Myc-tagged POP1 or Myc-tagged ASC, and the ability of ASC to co-immunoprecipitate with these proteins was tested. Consistent with the *in vitro* binding data, the five core mutations (E13A, K21A, R41A, D48A, and D51A) all disrupted the ability of ASC to co-immunoprecipitate with NLRP3 and POP1 (Fig. 2, *A* and *B*). An E67A mutation that did not affect interactions of the ASC PYD *in vitro* also did not disrupt co-immunoprecipitation of ASC with NLRP3 and POP1 (Fig. 2, *A* and *B*). When interaction with Myc-tagged full-length ASC was examined, although the ASC mutants showed diminished binding compared with wild-type ASC (Fig. 2*C*), some interaction was retained. Because the CARD domain of ASC is known to contribute to ASC self-association (32), it is likely that the CARD-mediated interaction allows partial retention of ASC self-association. To eliminate CARD-mediated effects, the ability of wild-type or mutant full-length ASC to co-immunoprecipitate with Myc-tagged ASC PYD was tested. These data showed the core mutations (E13A, K21A, R41A, D48A, and D51A) completely abolished the interaction between full-length ASC and Myc-tagged ASC PYD, although the E67A mutant retained interaction (Fig. 2*D*).

We noted that there was a variation in the level of ASC in the soluble cell lysates, with cells expressing wild-type ASC or the E67A mutant having the lowest levels. However, the expression levels of ASC in the total cell lysates were similar (supplemental Fig. S1). Because ASC forms aggregates *in vivo* (35), we surmise that a large fraction of wild-type and E67A ASC form insoluble aggregates, whereas the binding-defective ASC mutants are more soluble because of decreased self-association. This is consistent with previous studies using fluorescence microscopy to demonstrate that mutations K21A, R41A, D48A, and D51A are defective in ASC filament formation (31). Similarly, the
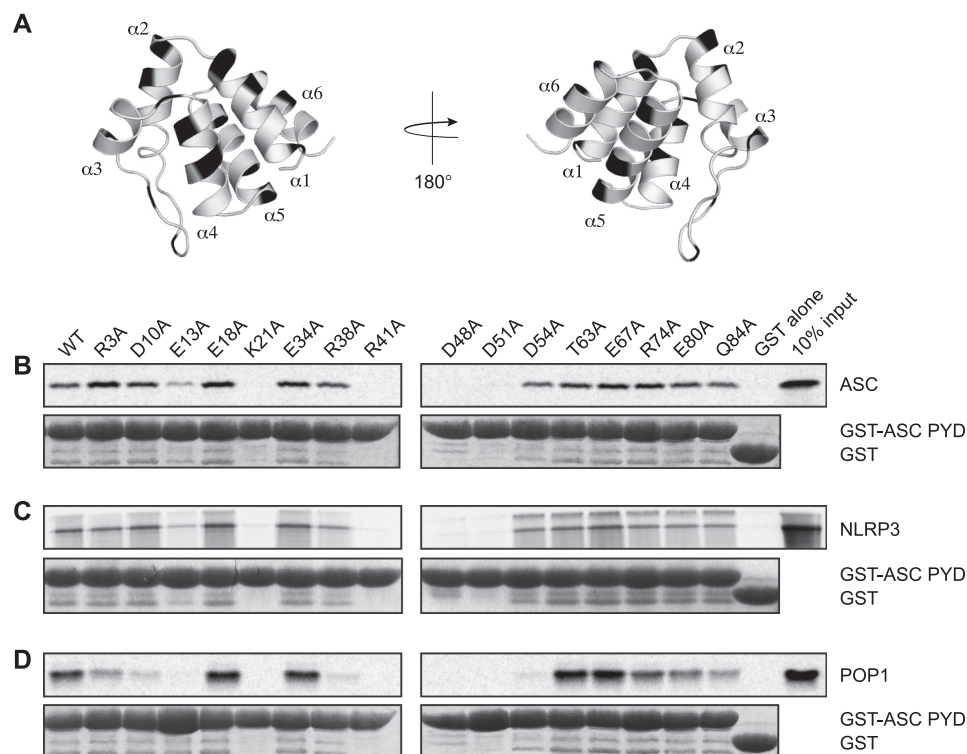
FIGURE 1. **Identification of residues important for ASC PYD interactions.** *A*, ribbon representation of the ASC PYD structure (Protein Data Bank ID code 1UCP) (37) with locations of the residues mutated in this study indicated. The residues mutated include Arg-3, Asp-10, and Glu-13 (helix α1); Glu-18 and Lys-21 (helix α2); Glu-34 and Arg-38 (α2-α3 loop); Arg-41 (helix α3); Asp-48 (α3-α4 loop); Asp-51 and Asp-54 (helix α4); Thr-63, Glu-67, and Arg-74 (helix α5); and Glu-80 and Gln-84 (helix α6). *B–D*, purified bead-bound wild-type or mutant GST-ASC PYD or GST alone were used in binding assays with *in vitro* translated [^{35}S]methionine-labeled ASC (*B*), NLRP3 (*C*), or POP1 (*D*). Bound protein was eluted with SDS-PAGE sample buffer and subjected to SDS-PAGE. GST-ASC PYD was detected by Coomassie stain, whereas ^{35}S-labeled proteins were detected by phosphorimaging. An amount representing 10% of the input of *in vitro* translated protein used for binding studies is shown. Note that the upper band in the lanes containing NLRP3 is attributed to formation of a high molecular weight aggregate.

reduced level of FLAG-tagged NLRP3 in the soluble lysate from cells expressing wild-type or E67A ASC is likely due to the formation of insoluble complexes of NLRP3 with wild-type or E67A ASC and to a much lesser extent with the binding-defective ASC mutants. This is consistent with the formation of large complexes of NLRP3 and ASC upon co-expression in HEK 293T cells that have been observed by microscopy (50).

ASC PYD Contains Two Distinct Binding Sites—Of the five key residues important for interactions mediated by the ASC PYD, two residues (Lys-21 and Arg-41) are located in helices α2 and α3 (Fig. 3*A*), and cluster within a positively charged surface (Fig. 3*B*). The other three residues (Glu-13, Asp-48, and Asp-51) are present in helix α1, α3-α4 loop, and helix α4 (Fig. 3*A*) and are located within a negatively charged surface (Fig. 3*B*). These two highly charged patches are adjacently located in the ASC PYD structure. The additional residues required for POP1 interaction (Arg-3, Asp-10, Arg-38, Asp-54, and Gln-84) are located close in sequence or in space to the key residues required for binding (Fig. 3*A*). Residues Asp-10 and Asp-54 are within the negatively charged patch, whereas Arg-38 is part of the positively charged surface (Fig. 3*B*). Residues Arg-3 and Gln-84, which have mild effects on POP1 interaction when mutated, are located on the periphery of the negatively charged binding surface.

Because the residues selected for mutagenesis were highly surface exposed, the mutations were not expected to disrupt

the structure of the ASC PYD. However, we could not discount effects on protein conformation, and therefore we assessed the structural integrity of the ASC PYD mutants that affected interactions using NMR spectroscopy. ^{15}N-Labeled wild-type and mutant ASC PYDs were analyzed by comparing their two-dimensional ^{1}H-^{15}N HSQC spectra (supplemental Fig. S2). The peaks corresponding to each residue in wild-type ASC PYD were assigned using standard triple resonance experiments (46) and are labeled in supplemental Fig. S2*A*. Comparison of the HSQC spectra of the binding-deficient mutants (E13A, K21A, R41A, D48A, and D51A) with wild-type ASC PYD demonstrated that the mutant proteins are correctly folded, with only minor shifts in the peaks of residues that are close in sequence or space to the mutation sites (supplemental Fig. S2, *B–F*). For example, the K21A mutation in helix α2 induced very small shifts ($\Delta\delta < 0.005$ ppm) in residues Glu-18, Leu-20, Phe-23, Lys-24, Leu-25, and Leu-27, which are close in sequence, as well as in residues Ala-43, Leu-44, Leu-45, Ser-46, and Asp-48, which are close in space on helix α3 and the α3-α4 loop.

NMR analysis of the additional ASC PYD mutants (R3A, D10A, R38A, and D54A) that affected interaction with POP1 showed that the R3A, D10A, and D54A mutations only induced minor shifts in a few residues that were close to the mutation site (supplemental Fig. S3, *A, B, and D*). However, the R38A mutation in the α2-α3 loop caused numerous shifts as well as the disappearance of several peaks (supplemental Fig. S3*C*) that
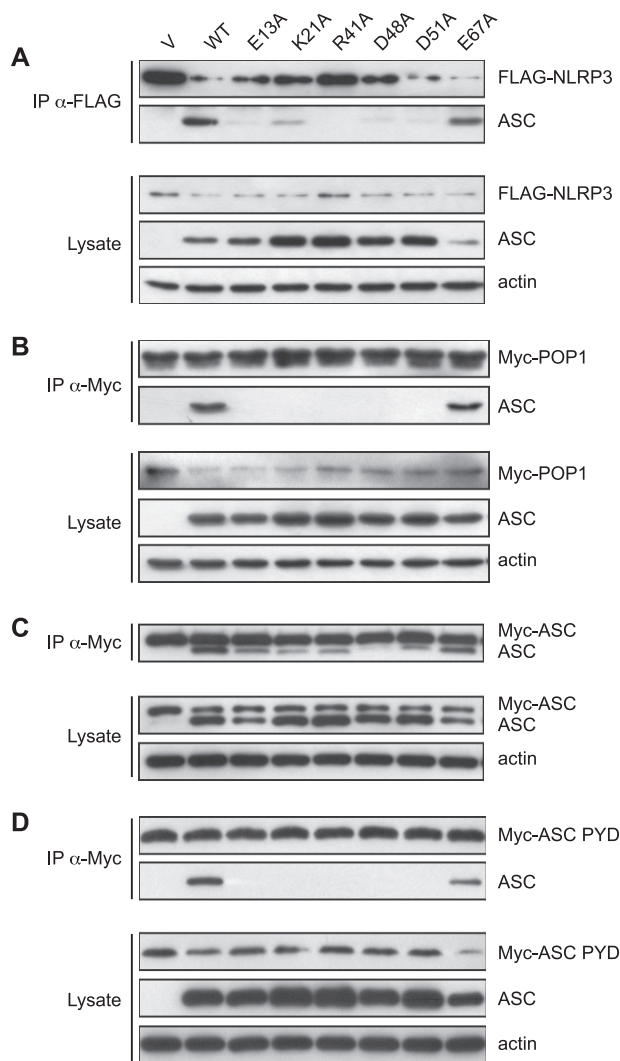
FIGURE 2. **Validation of key residues for ASC PYD interactions in mammalian cell lysates.** Plasmids expressing WT or mutant ASC or empty vector (V) were co-transfected with plasmids expressing either FLAG-tagged NLRP3 (A), Myc-tagged POP1 (B), Myc-tagged full-length ASC (C), or Myc-tagged ASC PYD (D) in HEK 293T cells. FLAG- or Myc-tagged proteins were immunoprecipitated (IP) with appropriate antibodies, and the immunoprecipitated complexes were analyzed by Western blotting. NLRP3 was detected using an anti-FLAG antibody, POP1 was detected using an anti-Myc antibody, full-length ASC was detected using an anti-ASC antibody, and Myc-tagged ASC PYD was detected using an anti-Myc antibody. The level of β-actin was used as an internal loading control and was detected using an anti-β-actin antibody.
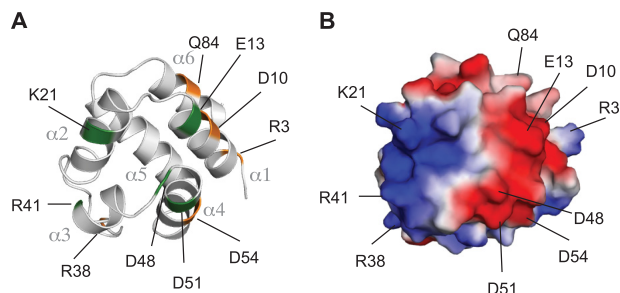

FIGURE 3. **Residues required for interaction of the ASC PYD map to positive and negative surfaces.** Mutations that diminish interactions of the ASC PYD were mapped onto ribbon representation (A) and surface electrostatic potential (B) of the ASC PYD structure (Protein Data Bank ID code 1UCP) (37). In A, mutations that diminished all interactions are shown in *green*, whereas mutations that only diminish interaction with POP1 are shown in *orange*.
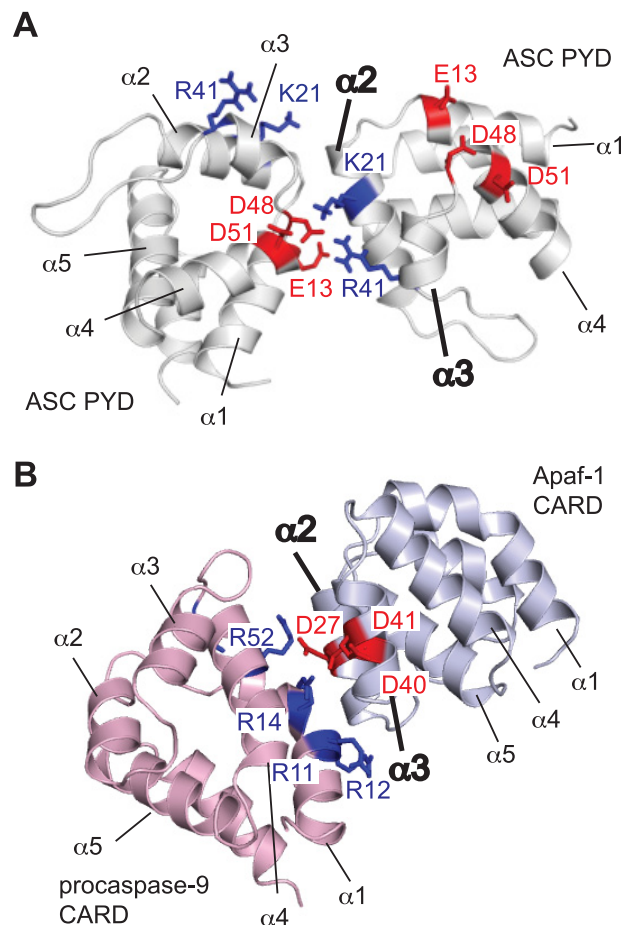

FIGURE 4. **Model of the ASC PYD homodimer in comparison with the Apaf-1·procaspase-9 CARD complex.** A, model of the ASC PYD homodimer generated using HADDOCK. B, model of the Apaf-1·procaspase-9 CARD complex (Protein Data Bank ID code 3YGS) (52). In both A and B, the subunit using helices α2 and α3 for interaction is shown in a similar orientation. Acidic (*red*) and basic residues (*blue*) important for interaction are indicated.

mainly correspond to residues in helices α4 and α5, which are in contact with the α2-α3 loop. This suggests a structural perturbation in the vicinity of the mutation.

NMR studies of ASC PYD were undertaken at pH 4 because the protein has a tendency to self-associate and aggregate at neutral pH (37). Low pH conditions gave rise to a monomeric species as indicated by uniform narrow line widths in the HSQC spectra (supplemental Fig. S2). Attempts to further validate the residues important for ASC interactions using NMR chemical shift mapping at neutral pH were unsuccessful because of precipitation of ASC PYD.

Binding Mode of the ASC PYD—We postulate that the two binding sites with opposing charges (Fig. 3B) interact to mediate ASC self-association. To generate a model for dimerization of ASC PYD, we used the molecular docking program HADDOCK (48). Residues on the positively charged surface (Lys-21 and Arg-41) were defined as active residues for one ASC PYD molecule, whereas residues on the negatively charged surface (Glu-13, Asp-48, and Asp-51) were designated active residues for the second molecule. All of these residues are surface-exposed (>27% solvent accessibility), and alanine mutation of
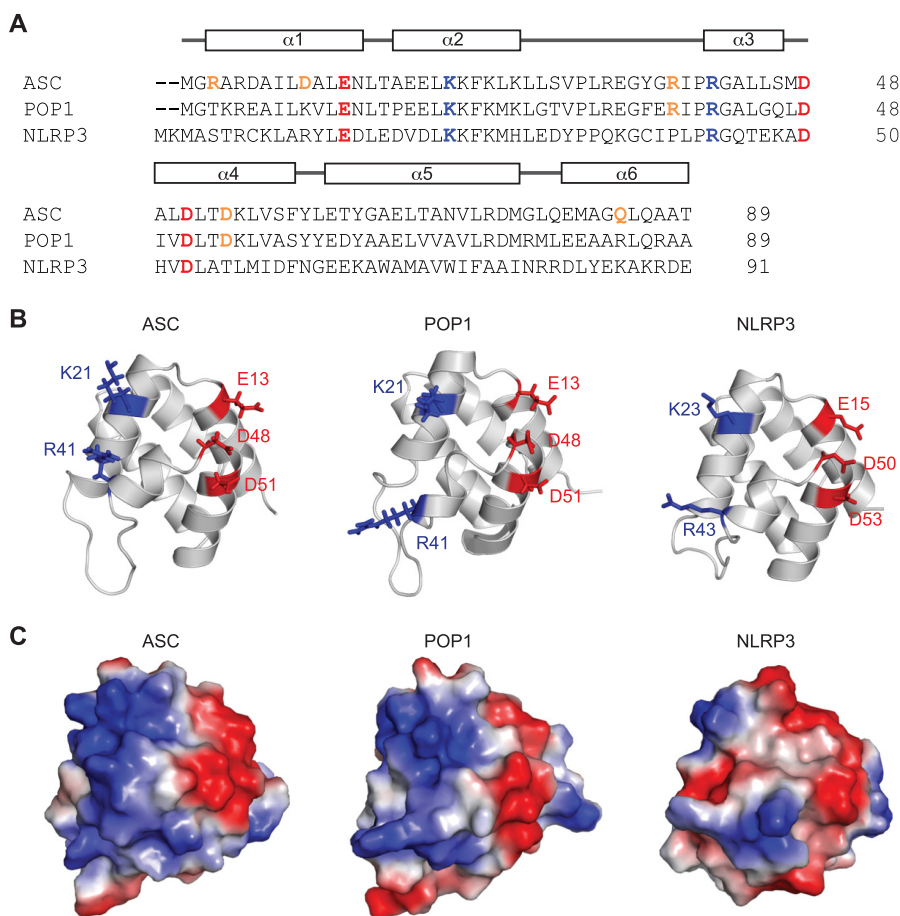
FIGURE 5. **Residues critical for interaction of the ASC PYD are conserved in NLRP3 and POP1.** *A*, amino acid sequence alignment of the PYDs of ASC, POP1, and NLRP3. Basic and acidic residues important for all interactions of the ASC PYD are colored *blue* and *red*, respectively, whereas additional residues important for interaction with POP1 are colored *orange*. *B*, structures of the PYDs of ASC (Protein Data Bank ID code 1UCP) (37), POP1 (Protein Data Bank ID code 2HM2) (42), and NLRP3 (Protein Data Bank ID code 3QF2) (39) were aligned using PyMOL, and the residues important for interaction of the ASC PYD are indicated with acidic residues in *red* and basic residues in *blue*. *C*, surface electrostatic potential of the PYDs of ASC, POP1, and NLRP3 shown in the same orientation as *B*.

these residues disrupted interaction without any effect on structure.

Analysis of the ASC PYD homodimer model (Fig. 4*A*) using PISA (51) showed that the interface comprises Glu-18, Lys-21, Lys-22, Leu-25, Lys-26, Arg-41, and Met-76 from one molecule and Glu-13, Thr-16, Ala-17, Lys-24, Ser-46, Asp-48, Ala-49, Leu-50, and Asp-51 from the second molecule. The interaction appears to be dominated by electrostatic contacts and hydrogen bonding with a smaller contribution from hydrophobic side chains. Overall the observed interactions are in good agreement with the mutagenesis data. Interestingly, the structure resembles the CARD interaction between Apaf-1 and procaspase-9 (Fig. 4*B*) in which helices α2 and α3 of Apaf-1 interact with helices α1 and α4 of procaspase-9 (52). However, there are some differences between the PYD and CARD complexes because of structural differences between the CARD and PYD domains. In CARD domains, helix 1 is bent, and this allows the procaspase-9 CARD to mediate a greater contact area with helices α2 and α3 of Apaf-1 (Fig. 4*B*). Consistent with this, the buried surface area of the CARD complex is 1100 Å^2, whereas the buried surface area of the ASC PYD homodimer is 636 Å^2. In addition, the orientation of helices α2 and α3 are almost parallel to helices α1 and α4 in the CARD complex, but in the

ASC PYD homodimer helices α2 and α3 are perpendicular to helices α1 and α4. Thus in the PYD complex only the C terminus of helix α1 and the N terminus of helix α4 of one PYD contact helices α2 and α3 of the second PYD. Interestingly, the docking model shows that the PYDs of the homodimer are oriented to enable the two interaction sites of each subunit to engage in further independent interactions (Fig. 4*A*) either to build a higher order ASC oligomer or to interact with other binding proteins.

Residues Important for ASC PYD Interactions Are Conserved in NLRP3 and POP1—The key residues for ASC PYD self-association, as well as interaction with NLRP3 and POP1, are shared, suggesting that the mode of interaction of ASC PYD with NLRP3 and POP1 is similar to the mode of self-association. To investigate this further, we performed a sequence alignment of the PYDs of ASC, POP1, and NLRP3 to ascertain whether the residues important for interactions of the ASC PYD are conserved (Fig. 5*A*). Notably, all five key residues are identical in the PYDs of NLRP3 and POP1. Furthermore, a structural alignment of the ASC, POP1, and NLRP3 PYDs showed that the spatial arrangement of these residues in the structures is very similar (Fig. 5*B*). These data are consistent with a conserved binding mode of the ASC PYD with these

PYDs. There are, however, some differences in the surface electrostatics of these different PYDs. In particular, the positive surface of NLRP3 is markedly less contiguous (Fig. 5*C*). The differences in electrostatics and shape of the PYDs are likely to dictate their binding specificity.

ASC Self-association Promotes Interaction with NLRP3 but Inhibits Interaction with POP1—Because the residues on ASC PYD that were important for self-association were also required for interaction with NLRP3 and POP1, we tested whether self-association of the ASC PYD is compatible with NLRP3 or POP1 binding. Bead-bound GST-ASC PYD was incubated with *in vitro* translated NLRP3 or POP1 alone or in the presence of increasing concentrations of soluble ASC PYD. As expected, there was increased self-association of the soluble ASC PYD with the bead-bound GST-ASC PYD as the concentration of soluble ASC PYD was increased. The binding of POP1 to bead-bound GST-ASC PYD was diminished in the presence of self-associated ASC PYD (Fig. 6*A*), which is consistent with POP1 and soluble ASC PYD competing for interaction with GST-ASC PYD. In contrast, interaction of NLRP3 with GST-ASC PYD appeared to be promoted in the presence of self-associated ASC PYD (Fig. 6*B*). The increased binding of NLRP3 in the presence of self-associated ASC PYD was more evident when an increased amount of bead-bound GST-ASC PYD and soluble ASC PYD were used in the assay (Fig. 6*C*). There was some precipitation of soluble ASC PYD, based on nonspecific binding to GST when the highest amount of soluble ASC PYD was used (26 μg of ASC PYD; Fig. 6*C*). Interestingly, the precipitated ASC PYD aggregates could also mediate interaction with NLRP3. However, this was insignificant compared with the increased interaction with NLRP3 that was mediated by self-association of ASC with GST-ASC PYD. These data are consistent with oligomerized ASC PYD interacting with NLRP3.

ASC Interaction with NLRP3 Is Retained in the Presence of POP1—Although POP1 is proposed to function as a modulator of the inflammasome (33), the effect of POP1 on interaction of ASC with NLRP3 has not been tested. Because the ASC PYD appears to use the same residues to interact with POP1 and NLRP3 (Fig. 1), POP1 may inhibit interaction between ASC PYD and NLRP3. To test this hypothesis, bead-bound GST-ASC PYD was incubated with *in vitro* translated NLRP3 in the presence of increasing concentrations of purified recombinant POP1. No decrease in the amount of NLRP3 bound to GST-ASC PYD was observed even in the presence of a 10-fold excess of POP1 compared with GST-ASC PYD (Fig. 7, *A* and *B*). In contrast, the binding of NLRP3 to bead-bound GST-ASC PYD was decreased in the presence of purified Pyrin PYD (Fig. 7*C*). This is consistent with previous studies showing that Pyrin can inhibit the interaction between ASC and NLRP3 (53). In an alternative approach, we co-expressed NLRP3 and ASC in HEK 293T cells in the presence or absence of POP1 and tested the ability of ASC to co-immunoprecipitate with NLRP3. In agreement with the GST pull-down assay, POP1 did not inhibit the ability of ASC to co-immunoprecipitate with NLRP3 (Fig. 7*D*).
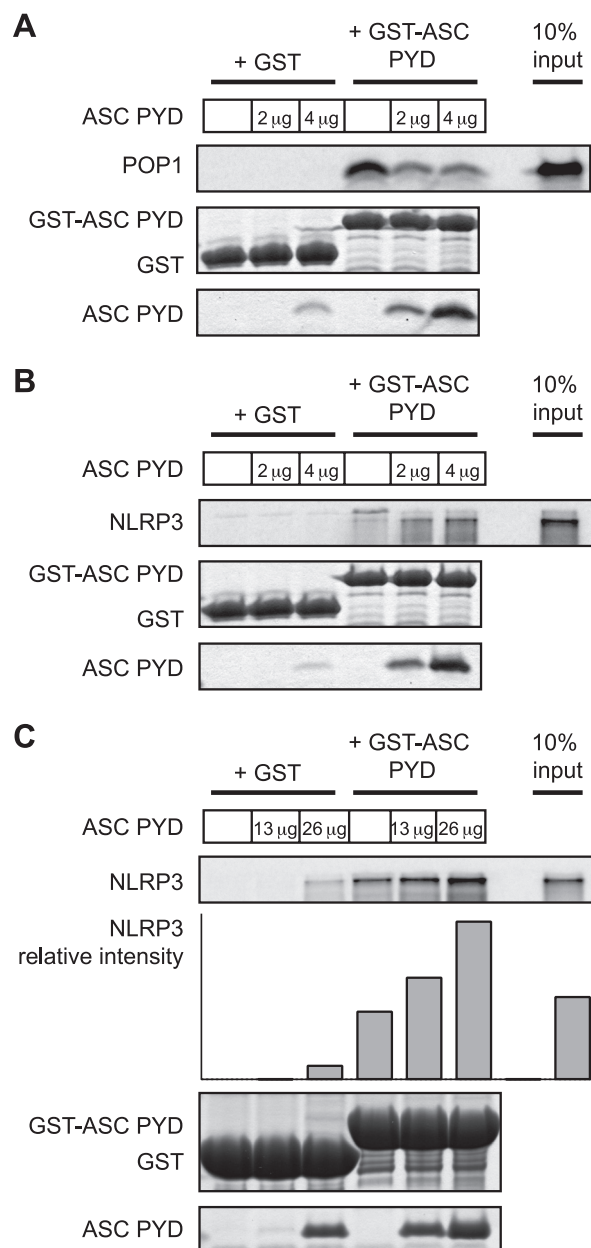

FIGURE 6. **ASC self-association promotes interaction with NLRP3 but not with POP1.** Purified bead-bound GST-ASC PYD or GST alone were used for binding assays with soluble ASC PYD (2 or 4 μg) and either *in vitro* translated [^{35}S]methionine-labeled POP1 (*A*) or NLRP3 (*B*). The final volume of the binding reactions was 150 μl. *C*, purified bead-bound GST-ASC PYD or GST alone were used for binding assays with soluble ASC PYD (13 or 26 μg) and *in vitro* translated [^{35}S]methionine-labeled NLRP3. The final volume of the binding reactions was 1 ml, and 10 times more bead-bound protein than in *A* and *B* was used. In *A*–*C*, bound proteins were eluted with SDS-PAGE sample buffer and subjected to SDS-PAGE. GST, GST-ASC PYD, and soluble ASC PYD were detected by Coomassie stain, whereas ^{35}S-labeled proteins were detected by phosphorimaging. An amount representing 10% of the input of *in vitro* translated protein used for binding studies is shown.

DISCUSSION

Assembly of oligomeric complexes that function in inflammatory and apoptotic signaling pathways is largely mediated by protein interaction domains of the death fold superfamily (28, 29). These domains mediate the recruitment of effector molecules, such as caspases and kinases, to oligomeric platforms allowing them to come into close proximity to gain activity
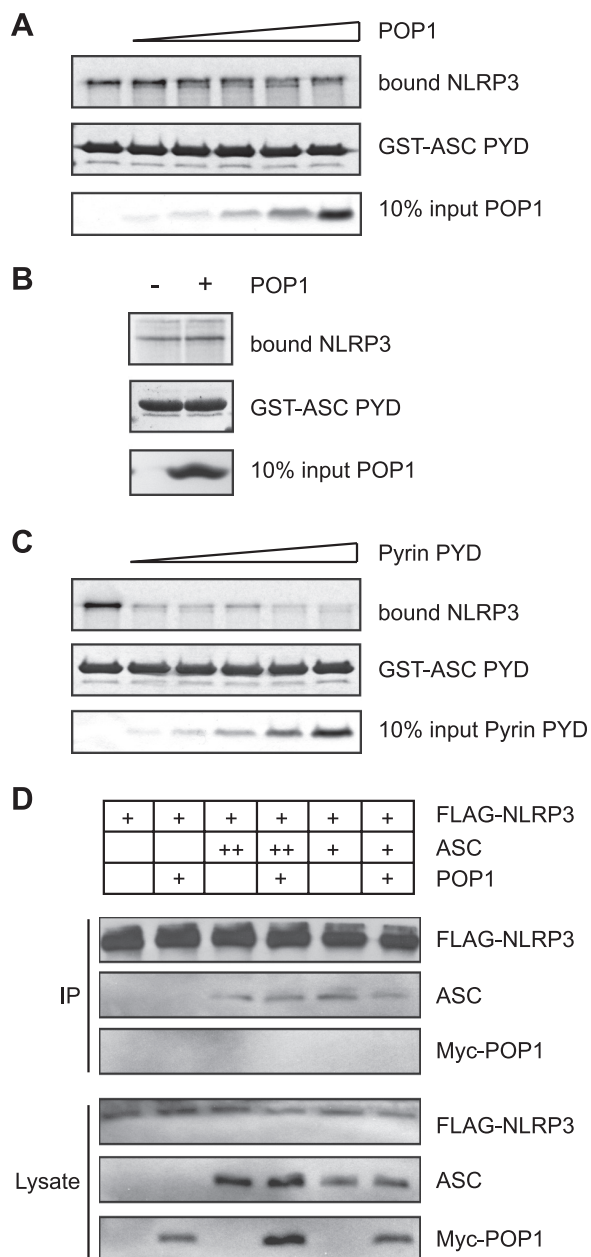
FIGURE 7. POP1 does not inhibit interaction of ASC with NLRP3. *A–C*, purified bead-bound wild-type or mutant GST-ASC PYD was incubated with *in vitro* translated [^{35}S]methionine-labeled NLRP3 alone or in the presence of increasing concentrations of purified POP1 (*A* and *B*) or purified Pyrin PYD (*C*). Bound protein was eluted with SDS-PAGE sample buffer and subjected to SDS-PAGE. GST-ASC PYD, purified POP1, and purified Pyrin PYD were detected by Coomassie stain, whereas ^{35}S-labeled proteins were detected by phosphorimaging. *D*, ASC was co-expressed with FLAG-tagged NLRP3 in the presence or absence of Myc-tagged POP1. Cells were transfected with two different concentrations of ASC to increase the probability of detecting an effect. NLRP3 was immunoprecipitated (*IP*) with an anti-NLRP antibody, and the immunoprecipitated complexes were analyzed by Western blotting. NLRP3 was detected using an anti-FLAG antibody, POP1 was detected using an anti-Myc antibody, and full-length ASC was detected using an anti-ASC antibody.

(54–56). The NLRP3 inflammasome is assembled via PYD and CARD interactions to promote caspase-1 activation (7), but its structure is poorly characterized. ASC is a critical adaptor protein that bridges the interaction between the NLRP3 oligomer and procaspase-1 (7). ASC also self-associates to form a

caspase-1-activating platform termed the pyroptosome (36). To gain insights into the interaction modes of PYDs and the molecular architecture of the inflammasome and pyroptosome complexes, we investigated the molecular basis of ASC PYD interactions. The binding surfaces of ASC PYD required for self-association, recruitment to NLRP3, and interaction with POP1 were identified using site-directed mutagenesis. Residues Glu-13, Asp-48, and Asp-51 in the negatively charged surface and residues Lys-21 and Arg-41 in the positively charged surface of ASC PYD were critical for all three interactions. Because the two charged surfaces are located on opposite sides of ASC PYD, there are at least two distinct binding sites that mediate interactions. Furthermore, we show that ASC PYD can use these two sites to simultaneously engage in self-association and interaction with NLRP3.

Construction of a model for the homodimeric complex between ASC PYDs revealed how residues Lys-21 and Arg-41 in helices α2 and α3 of one PYD interact with residues Glu-13, Asp-48, and Asp-51 in helix α1, the α3-α4 loop, and helix α4 of another PYD. Notably, these residues are conserved in ASC from diverse species (supplemental Fig. S4), supporting an important role for these residues. The homodimer interface resembles a type I interaction, which is one of three conserved interaction types found in complexes formed by domains of the death fold superfamily (29). The type I interaction was originally described for the Apaf-1·procaspase-9 CARD complex (52) and has subsequently been found between DD subunits in other complexes including the PIDDosome, a caspase-2-activating complex assembled in response to DNA damage (54), and the Myddosome assembled during Toll-like receptor signaling (55), as well as the Fas·FADD complex formed during death receptor signaling (56). The type I interaction in these complexes mediates self-association of DDs, as well as interactions with complementary DDs in binding partners.

Our finding that residues Asp-48 and Asp-51 in the negatively charged surface and residues Lys-21 and Arg-41 in the positively charged surface of the ASC PYD are important for self-association is in good agreement with a previous study showing that mutation of these residues prevented assembly of the ASC PYD into filaments (31). In contrast, we also identified a role for Glu-13 in helix α1 for ASC PYD self-association. However, the E13A mutation only partially disrupted self-association in our assay; thus it may not noticeably diminish filament formation *in vivo*. A second discrepancy between our data and the previous study is in the role of Leu-25, which was reported to be important for ASC PYD filament formation (31). Our study does not support a critical role for this residue, because Leu-25 can be replaced by alanine without affecting self-association (supplemental Fig. S5A). However, Leu-25 is spatially close to Lys-21 and Arg-41 (supplemental Fig. S5D) and potentially contacts other hydrophobic residues (Ala-49 and Leu-50) in the adjacent ASC PYD.

Interestingly, when we generated a model for oligomerization of the ASC PYD via the type I interface present in the homodimer model, we found that ASC PYDs form a helical-like arrangement with three PYDs per turn (Fig. 8). This complex can be extended to form a filament and explains the propensity
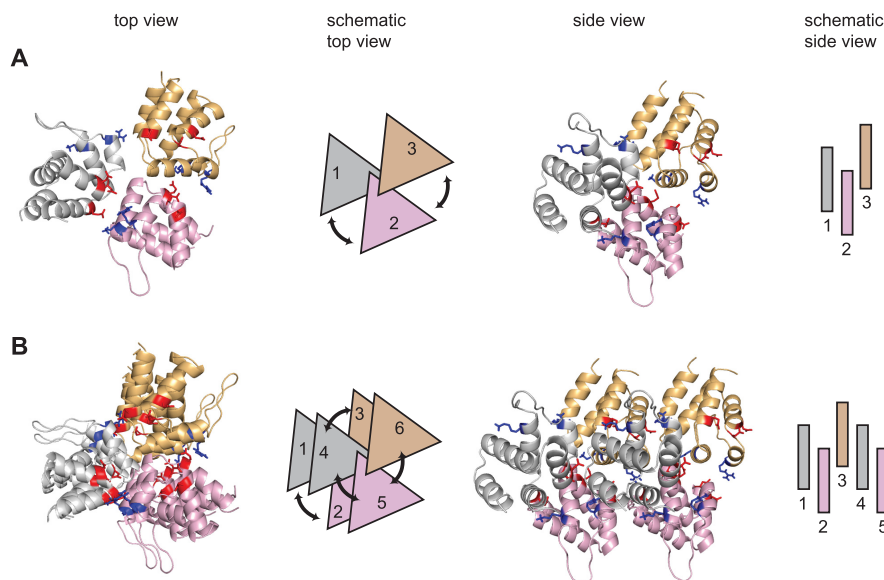
FIGURE 8. **Assembly of the ASC PYD into higher order oligomers.** To generate higher order ASC PYD oligomers, multiple copies of the ASC PYD homodimer model were aligned using the type I interface; subunit 2 of one homodimer was superimposed with subunit 1 of a second homodimer. *A*, trimeric complex of ASC PYDs. The three PYDs form one turn of a helix and individual PYDs are colored *gray*, *pink*, and *orange*, respectively. Top and side views of the complex are shown. Schematics of the top and side views are also shown to illustrate the helical arrangement of the complex. *B*, hexameric complex of ASC PYDs to illustrate extension into a filament. In both *A* and *B*, the *double-headed arrows* indicate the interactions between PYDs, and acidic and basic residues that mediate ASC PYD interactions are colored *red* and *blue*, respectively.

of the ASC PYD to form filaments *in vivo* (31, 32). Consistent with previous observations that full-length ASC also forms filamentous aggregates *in vivo* (32), we were also able to generate a hypothetical model of full-length ASC assembled into a filament via PYD interactions (supplemental Fig. S6). In this model, the CARD domains are oriented away from the ASC PYD filament and do not interfere with assembly. Because the CARD and PYD are separated by a flexible linker, the CARD is free to engage in independent interactions (57). In addition to interaction with procaspase-1, the CARDs may contribute to self-association and thus further stabilize the ASC filament. Assembly of ASC into such a filament is also in agreement with a previous study suggesting that the ASC pyroptosome is an oligomer of ASC dimers (36).

The interaction of ASC PYD with POP1 is likely to share a similar binding mode to ASC PYD self-association. POP1 has high sequence identity to ASC PYD (64%), and the genes encoding both proteins are proposed to have arisen by gene duplication (33). Moreover, POP1 binding and ASC self-association are competitive interactions. Our data based on *in vitro* GST pull-down assays as well as co-immunoprecipitation in HEK 293T cells clearly demonstrate that mutation of residues on both the positive and negative surfaces of ASC PYD also disrupt interaction with POP1. However, a previous study using NMR spectroscopy to map the surface of ASC PYD that interacts with POP1 proposed a role for residues Asp-6, Glu-13, Asp-48, and Asp-D54 on the negative surface but did not find any evidence of a role for residues in the positively charged surface (49). Notably, an L25A mutant was used in this study to improve the solubility of ASC PYD (49). However, our *in vitro* binding data show that the L25A mutation diminishes interaction of ASC PYD with POP1 (supplemental Fig. S5C); thus it is not surprising that only very small chemical shift changes ($\Delta\delta < 0.07$ ppm) were detected upon titration of ^{15}N-labeled ASC PYD (L25A)

with POP1. Interestingly, the same study (49) showed that mutagenesis of Lys-21 (K21A) and Arg-41 (R41W) in the positive surface also diminished interaction of ASC PYD with POP1. This observation was proposed to be via a transduced effect, whereby conformational changes at one surface are communicated to the other surface through the hydrophobic core. However, our data indicate that R41A and K21A mutations do not perturb the structure, suggesting that residues in the positive surface of ASC PYD also directly interact with POP1. We postulate that POP1 can interact with both surfaces of the ASC PYD in the same manner that ASC PYD forms a filament, and thus POP1 is likely to insert into an ASC filament. In support of this hypothesis, POP1 is recruited to ASC specks when co-expressed with ASC (33).

In contrast to the competitive nature of POP1 binding, ASC self-association promotes NLRP3 interaction. This observation raises the possibility that mutations disrupting ASC PYD self-association may indirectly disrupt interaction with NLRP3. However, no additional mutations in ASC PYD disrupt interaction with NLRP3, and residues important for ASC PYD interactions are conserved in NLRP3 PYD. These observations suggest a similar binding mode to the ASC PYD homodimer. Moreover, because each ASC PYD of the homodimer retains an available interaction site, ASC PYD self-association and interaction with NLRP3 are not mutually exclusive. Indeed, we generated a model that demonstrates how the ASC PYD homodimer can interact with two NLRP3 PYDs (supplemental Fig. S7). The ability of ASC PYDs to self-associate while interacting with NLRP3 is expected to allow the ASC CARD domains to recruit procaspase-1 and induce its activation. Although our model explains how the ASC PYD can self-associate and interact with NLRP3 PYDs, detailed mapping of interaction sites on NLRP3 PYD are required to validate the model.

The differential effects of ASC self-association on interaction with NLRP3 and POP1 are likely due to the oligomerization states of NLRP3 and POP1. Because NLRP3 assembles into an oligomer (6), its interaction with ASC PYD is likely to be promoted by self-association because of increased contacts between self-associated ASC and the NLRP3 oligomer as in our model. However, because POP1 is a monomer (42), ASC self-association does not promote its interaction. The fact that overlapping sites on ASC PYD interact with POP1 and NLRP3 suggested that POP1 may inhibit interaction of ASC with NLRP3. However, we found that addition of POP1 had no effect on the interaction between ASC and NLRP3. POP1 may have a lower affinity for ASC than NLRP3 and thus may not function as an inhibitor of inflammasome assembly. In agreement with our data, previous studies have shown that POP1 does not inhibit IL-1β secretion upon co-expression with NLRP3, ASC, and procaspase-1 but instead promotes it (33). Moreover, because ASC is known to interact with the IKK complex (58), POP1 may modulate this other aspect of ASC function.

The residues important for ASC PYD interaction are not all conserved in the PYDs of NLRP1, NLRP7, NLRP10, and NLRP12 (supplemental Fig. S8, *A* and *B*). However, the PYDs of NLRP7, NLRP10, and NLRP12 do contain positively and negatively charged patches at similar locations, although they are less pronounced (supplemental Fig. S8*C*). For example, in the NLRP7 and NLRP12 PYDs, a hydrophobic patch interrupts the positive surface (supplemental Fig. S8*C*). Nonetheless, both NLRP7 and NLRP12 appear to retain the ability to interact with ASC (9, 59). The electrostatic surface of NLRP1 is considerably different from that of the ASC PYD (supplemental Fig. S8*C*); nonetheless it also binds ASC (6). In addition, although POP1 and NLRP3 contain the core residues required for ASC PYD interaction, they do not interact with each other (Fig. 7*D*). This suggests that additional residues surrounding the core interaction sites identified here will modulate interactions and direct specificity. Therefore, although this study has given critical insights into the interaction mode of the PYD, additional studies will be required to fully understand the range of interaction modes mediated by PYDs.

Because a single binding site on the ASC PYD is insufficient to mediate a stable interaction with a binding partner, this suggests that PYD interactions are low affinity individual interactions that are strengthened upon oligomerization to increase binding avidity. The requirement for protein oligomerization is a recurring theme in the assembly of complexes mediated by members of the death fold superfamily such as the apoptosome (60), PIDDosome (54), Myddosome (55), and Fas·FADD DD complex (56). In each case, an oligomeric platform recruits successive components. For example, the apoptosome is built upon heptameric Apaf-1, which has a much higher affinity for procaspase-9 than the isolated Apaf-1 CARD (61). Similarly, during assembly of the Myddosome, MyD88 is recruited by activated Toll-like receptors and upon oligomerization recruits IRAK4 (62). The ability of ASC to self-associate and interact with NLRP3 indicates that ASC self-association may promote clustering of downstream recruited procaspase-1 as observed in other complexes where components cluster to allow activation of the terminally recruited effector molecules (63). Thus our study identifies many similarities between the roles of the PYD and other death fold domains in the assembly and activation of oligomeric signaling complexes.

REFERENCES

1. Meylan, E., Tschopp, J., and Karin, M. (2006) Intracellular pattern recognition receptors in the host response. *Nature* **442,** 39–44
2. Takeuchi, O., and Akira, S. (2010) Pattern recognition receptors and inflammation. *Cell* **140,** 805–820
3. Ting, J. P., Duncan, J. A., and Lei, Y. (2010) How the noninflammasome NLRs function in the innate immune system. *Science* **327,** 286–290
4. Davis, B. K., Wen, H., and Ting, J. P. (2011) The inflammasome NLRs in immunity, inflammation, and associated diseases. *Annu. Rev. Immunol.* **29,** 707–735
5. Poyet, J. L., Srinivasula, S. M., Tnani, M., Razmara, M., Fernandes-Alnemri, T., and Alnemri, E. S. (2001) Identification of Ipaf, a human caspase-1-activating protein related to Apaf-1. *J. Biol. Chem.* **276,** 28309–28313
6. Martinon, F., Burns, K., and Tschopp, J. (2002) The inflammasome. A molecular platform triggering activation of inflammatory caspases and processing of proIL-β. *Mol. Cell* **10,** 417–426
7. Agostini, L., Martinon, F., Burns, K., McDermott, M. F., Hawkins, P. N., and Tschopp, J. (2004) NALP3 forms an IL-1β-processing inflammasome with increased activity in Muckle-Wells autoinflammatory disorder. *Immunity* **20,** 319–325
8. Bruey, J. M., Bruey-Sedano, N., Newman, R., Chandler, S., Stehlik, C., and Reed, J. C. (2004) PAN1/NALP2/PYPAF2, an inducible inflammatory mediator that regulates NF-κB and caspase-1 activation in macrophages. *J. Biol. Chem.* **279,** 51897–51907
9. Khare, S., Dorfleutner, A., Bryan, N. B., Yun, C., Radian, A. D., de Almeida, L., Rojanasakul, Y., and Stehlik, C. (2012) An NLRP7-containing inflammasome mediates recognition of microbial lipopeptides in human macrophages. *Immunity* **36,** 464–476
10. Li, P., Allen, H., Banerjee, S., Franklin, S., Herzog, L., Johnston, C., McDowell, J., Paskind, M., Rodman, L., and Salfeld, J. (1995) Mice deficient in IL-1β-converting enzyme are defective in production of mature IL-1β and resistant to endotoxic shock. *Cell* **80,** 401–411
11. Gu, Y., Kuida, K., Tsutsui, H., Ku, G., Hsiao, K., Fleming, M. A., Hayashi, N., Higashino, K., Okamura, H., Nakanishi, K., Kurimoto, M., Tanimoto, T., Flavell, R. A., Sato, V., Harding, M. W., Livingston, D. J., and Su, M. S. (1997) Activation of interferon-γ inducing factor mediated by interleukin-1β converting enzyme. *Science* **275,** 206–209
12. Schroder, K., and Tschopp, J. (2010) The inflammasomes. *Cell* **140,** 821–832
13. Hoffman, H. M., and Brydges, S. D. (2011) Genetic and molecular basis of inflammasome-mediated disease. *J. Biol. Chem.* **286,** 10889–10896
14. Martinon, F., Agostini, L., Meylan, E., and Tschopp, J. (2004) Identification of bacterial muramyl dipeptide as activator of the NALP3/cryopyrin inflammasome. *Curr. Biol.* **14,** 1929–1934
15. Martinon, F., Pétrilli, V., Mayor, A., Tardivel, A., and Tschopp, J. (2006) Gout-associated uric acid crystals activate the NALP3 inflammasome. *Nature* **440,** 237–241
16. Mariathasan, S., Weiss, D. S., Newton, K., McBride, J., O'Rourke, K., Roose-Girma, M., Lee, W. P., Weinrauch, Y., Monack, D. M., and Dixit, V. M. (2006) Cryopyrin activates the inflammasome in response to toxins and ATP. *Nature* **440,** 228–232
17. Dostert, C., Pétrilli, V., Van Bruggen, R., Steele, C., Mossman, B. T., and

Tschopp, J. (2008) Innate immune activation through Nalp3 inflammasome sensing of asbestos and silica. *Science* **320,** 674–677

18. Eisenbarth, S. C., Colegio, O. R., O'Connor, W., Sutterwala, F. S., and Flavell, R. A. (2008) Crucial role for the Nalp3 inflammasome in the immunostimulatory properties of aluminium adjuvants. *Nature* **453,** 1122–1126

19. Muruve, D. A., Pétrilli, V., Zaiss, A. K., White, L. R., Clark, S. A., Ross, P. J., Parks, R. J., and Tschopp, J. (2008) The inflammasome recognizes cytosolic microbial and host DNA and triggers an innate immune response. *Nature* **452,** 103–107

20. Gross, O., Thomas, C. J., Guarda, G., and Tschopp, J. (2011) The inflammasome. An integrated view. *Immunol. Rev.* **243,** 136–151

21. Leemans, J. C., Cassel, S. L., and Sutterwala, F. S. (2011) Sensing damage by the NLRP3 inflammasome. *Immunol. Rev.* **243,** 152–162

22. Duewell, P., Kono, H., Rayner, K. J., Sirois, C. M., Vladimer, G., Bauernfeind, F. G., Abela, G. S., Franchi, L., Nuñez, G., Schnurr, M., Espevik, T., Lien, E., Fitzgerald, K. A., Rock, K. L., Moore, K. J., Wright, S. D., Hornung, V., and Latz, E. (2010) NLRP3 inflammasomes are required for atherogenesis and activated by cholesterol crystals. *Nature* **464,** 1357–1361

23. Vandanmagsar, B., Youm, Y. H., Ravussin, A., Galgani, J. E., Stadler, K., Mynatt, R. L., Ravussin, E., Stephens, J. M., and Dixit, V. D. (2011) The NLRP3 inflammasome instigates obesity-induced inflammation and insulin resistance. *Nat. Med.* **17,** 179–188

24. Vilaysane, A., Chun, J., Seamone, M. E., Wang, W., Chin, R., Hirota, S., Li, Y., Clark, S. A., Tschopp, J., Trpkov, K., Hemmelgarn, B. R., Beck, P. L., and Muruve, D. A. (2010) The NLRP3 inflammasome promotes renal inflammation and contributes to CKD. *J. Am. Soc. Nephrol.* **21,** 1732–1744

25. Halle, A., Hornung, V., Petzold, G. C., Stewart, C. R., Monks, B. G., Reinheckel, T., Fitzgerald, K. A., Latz, E., Moore, K. J., and Golenbock, D. T. (2008) The NALP3 inflammasome is involved in the innate immune response to amyloid-β. *Nat. Immunol.* **9,** 857–865

26. Cook, G. P., Savic, S., Wittmann, M., and McDermott, M. F. (2010) The NLRP3 inflammasome, a target for therapy in diverse disease states. *Eur. J. Immunol.* **40,** 631–634

27. Masters, S. L., Latz, E., and O'Neill, L. A. (2011) The inflammasome in atherosclerosis and type 2 diabetes. *Sci. Transl. Med.* **3,** 1–7

28. Park, H. H., Lo, Y. C., Lin, S. C., Wang, L., Yang, J. K., and Wu, H. (2007) The death domain superfamily in intracellular signaling of apoptosis and inflammation. *Annu. Rev. Immunol.* **25,** 561–586

29. Kersse, K., Verspurten, J., Vanden Berghe, T., and Vandenabeele, P. (2011) The death-fold superfamily of homotypic interaction motifs. *Trends Biochem. Sci.* **36,** 541–552

30. Srinivasula, S. M., Poyet, J. L., Razmara, M., Datta, P., Zhang, Z., and Alnemri, E. S. (2002) The PYRIN-CARD protein ASC is an activating adaptor for caspase-1. *J. Biol. Chem.* **277,** 21119–21122

31. Moriya, M., Taniguchi, S., Wu, P., Liepinsh, E., Otting, G., and Sagara, J. (2005) Role of charged and hydrophobic residues in the oligomerization of the PYRIN domain of ASC. *Biochemistry* **44,** 575–583

32. Masumoto, J., Taniguchi, S., and Sagara, J. (2001) Pyrin N-terminal homology domain- and caspase recruitment domain-dependent oligomerization of ASC. *Biochem. Biophys. Res. Commun.* **280,** 652–655

33. Stehlik, C., Krajewska, M., Welsh, K., Krajewski, S., Godzik, A., and Reed, J. C. (2003) The PAAD/PYRIN-only protein POP1/ASC2 is a modulator of ASC-mediated nuclear-factor-κB and pro-caspase-1 regulation. *Biochem. J.* **373,** 101–113

34. Richards, N., Schaner, P., Diaz, A., Stuckey, J., Shelden, E., Wadhwa, A., and Gumucio, D. L. (2001) Interaction between pyrin and the apoptotic speck protein (ASC) modulates ASC-induced apoptosis. *J. Biol. Chem.* **276,** 39320–39329

35. Masumoto, J., Taniguchi, S., Ayukawa, K., Sarvotham, H., Kishino, T., Niikawa, N., Hidaka, E., Katsuyama, T., Higuchi, T., and Sagara, J. (1999) ASC, a novel 22-kDa protein, aggregates during apoptosis of human promyelocytic leukemia HL-60 cells. *J. Biol. Chem.* **274,** 33835–33838

36. Fernandes-Alnemri, T., Wu, J., Yu, J. W., Datta, P., Miller, B., Jankowski, W., Rosenberg, S., Zhang, J., and Alnemri, E. S. (2007) The pyroptosome. A supramolecular assembly of ASC dimers mediating inflammatory cell death via caspase-1 activation. *Cell Death Differ.* **14,** 1590–1604

37. Liepinsh, E., Barbals, R., Dahl, E., Sharipo, A., Staub, E., and Otting, G. (2003) The death-domain fold of the ASC PYRIN domain, presenting a basis for PYRIN/PYRIN recognition. *J. Mol. Biol.* **332,** 1155–1163

38. Hiller, S., Kohl, A., Fiorito, F., Herrmann, T., Wider, G., Tschopp, J., Grütter, M. G., and Wüthrich, K. (2003) NMR structure of the apoptosis- and inflammation-related NALP1 pyrin domain. *Structure* **11,** 1199–1205

39. Bae, J. Y., and Park, H. H. (2011) Crystal structure of NALP3 protein pyrin domain (PYD) and its implications in inflammasome assembly. *J. Biol. Chem.* **286,** 39528–39536

40. Pinheiro, A. S., Proell, M., Eibl, C., Page, R., Schwarzenbacher, R., and Peti, W. (2010) Three-dimensional structure of the NLRP7 pyrin domain. Insight into pyrin-pyrin-mediated effector domain signaling in innate immunity. *J. Biol. Chem.* **285,** 27402–27410

41. Pinheiro, A. S., Eibl, C., Ekman-Vural, Z., Schwarzenbacher, R., and Peti, W. (2011) The NLRP12 pyrin domain. Structure, dynamics, and functional insights. *J. Mol. Biol.* **413,** 790–803

42. Natarajan, A., Ghose, R., and Hill, J. M. (2006) Structure and dynamics of ASC2, a pyrin domain-only protein that regulates inflammatory signaling. *J. Biol. Chem.* **281,** 31863–31875

43. Hill, J. M. (2008) NMR screening for rapid protein characterisation in structural proteomics. *Methods Mol. Biol.* **426,** 437–446

44. Delaglio, F., Grzesiek, S., Vuister, G. W., Zhu, G., Pfeifer, J., and Bax, A. (1995) NMRPipe. A multidimensional spectral processing system based on UNIX pipes. *J. Biomol. NMR* **6,** 277–293

45. Vranken, W. F., Boucher, W., Stevens, T. J., Fogh, R. H., Pajon, A., Llinas, M., Ulrich, E. L., Markley, J. L., Ionides, J., and Laue, E. D. (2005) The CCPN data model for NMR spectroscopy. Development of a software pipeline. *Proteins* **59,** 687–696

46. Sattler, M., Schleucher, J., and Griesinger, C. (1999) Heteronuclear multidimensional NMR experiments for the structure determination of proteins in solution employing pulsed field gradients. *Prog. NMR Spectrosc.* **34,** 93–158

47. Pellecchia, M., Sebbel, P., Hermanns, U., Wüthrich, K., and Glockshuber, R. (1999) Pilus chaperone FimC-adhesin FimH interactions mapped by TROSY-NMR. *Nat. Struct. Biol.* **6,** 336–339

48. de Vries, S. J., van Dijk, M., and Bonvin, A. M. (2010) The HADDOCK web server for data-driven biomolecular docking. *Nat. Protoc.* **5,** 883–897

49. Srimathi, T., Robbins, S. L., Dubas, R. L., Chang, H., Cheng, H., Roder, H., and Park, Y. C. (2008) Mapping of POP1-binding site on pyrin domain of ASC. *J. Biol. Chem.* **283,** 15390–15398

50. Yu, J. W., Wu, J., Zhang, Z., Datta, P., Ibrahimi, I., Taniguchi, S., Sagara, J., Fernandes-Alnemri, T., and Alnemri, E. S. (2006) Cryopyrin and pyrin activate caspase-1, but not NF-κB, via ASC oligomerization. *Cell Death Differ.* **13,** 236–249

51. Krissinel, E., and Henrick, K. (2007) Inference of macromolecular assemblies from crystalline state. *J. Mol. Biol.* **372,** 774–797

52. Qin, H., Srinivasula, S. M., Wu, G., Fernandes-Alnemri, T., Alnemri, E. S., and Shi, Y. (1999) Structural basis of procaspase-9 recruitment by the apoptotic protease-activating factor 1. *Nature* **399,** 549–557

53. Dowds, T. A., Masumoto, J., Chen, F. F., Ogura, Y., Inohara, N., and Núñez, G. (2003) Regulation of cryopyrin/Pypaf1 signaling by pyrin, the familial Mediterranean fever gene product. *Biochem. Biophys. Res. Commun.* **302,** 575–580

54. Park, H. H., Logette, E., Raunser, S., Cuenin, S., Walz, T., Tschopp, J., and Wu, H. (2007) Death domain assembly mechanism revealed by crystal structure of the oligomeric PIDDosome core complex. *Cell* **128,** 533–546

55. Lin, S. C., Lo, Y. C., and Wu, H. (2010) Helical assembly in the MyD88-IRAK4-IRAK2 complex in TLR/IL-1R signalling. *Nature* **465,** 885–890

56. Wang, L., Yang, J. K., Kabaleeswaran, V., Rice, A. J., Cruz, A. C., Park, A. Y., Yin, Q., Damko, E., Jang, S. B., Raunser, S., Robinson, C. V., Siegel, R. M., Walz, T., and Wu, H. (2010) The Fas-FADD death domain complex structure reveals the basis of DISC assembly and disease mutations. *Nat. Struct. Mol. Biol.* **17,** 1324–1329

57. de Alba, E. (2009) Structure and interdomain dynamics of apoptosis-associated speck-like protein containing a CARD (ASC). *J. Biol. Chem.* **284,** 32932–32941

58. Stehlik, C., Fiorentino, L., Dorfleutner, A., Bruey, J. M., Ariza, E. M., Sagara, J., and Reed, J. C. (2002) The PAAD/PYRIN-family protein ASC is a

dual regulator of a conserved step in nuclear factor κB activation pathways. *J. Exp. Med.* **196,** 1605–1615

59. Wang, L., Manji, G. A., Grenier, J. M., Al-Garawi, A., Merriam, S., Lora, J. M., Geddes, B. J., Briskin, M., DiStefano, P. S., and Bertin, J. (2002) PYPAF7, a novel PYRIN-containing Apaf1-like protein that regulates activation of NF-κB and caspase-1-dependent cytokine processing. *J. Biol. Chem.* **277,** 29874–29880

60. Acehan, D., Jiang, X., Morgan, D. G., Heuser, J. E., Wang, X., and Akey, C. W. (2002) Three-dimensional structure of the apoptosome. Implications for assembly, procaspase-9 binding, and activation. *Mol. Cell* **9,** 423–432

61. Shiozaki, E. N., Chai, J., and Shi, Y. (2002) Oligomerization and activation of caspase-9, induced by Apaf-1 CARD. *Proc. Natl. Acad. Sci. U.S.A.* **99,** 4197–4202

62. George, J., Motshwene, P. G., Wang, H., Kubarenko, A. V., Rautanen, A., Mills, T. C., Hill, A. V., Gay, N. J., and Weber, A. N. (2011) Two human *MYD88* variants, S34Y and R98C, interfere with MyD88-IRAK4-Myddosome assembly. *J. Biol. Chem.* **286,** 1341–1353

63. Ferrao, R., and Wu, H. (2012) Helical assembly in the death domain (DD) superfamily. *Curr. Opin. Struct. Biol.* **22,** 241–247
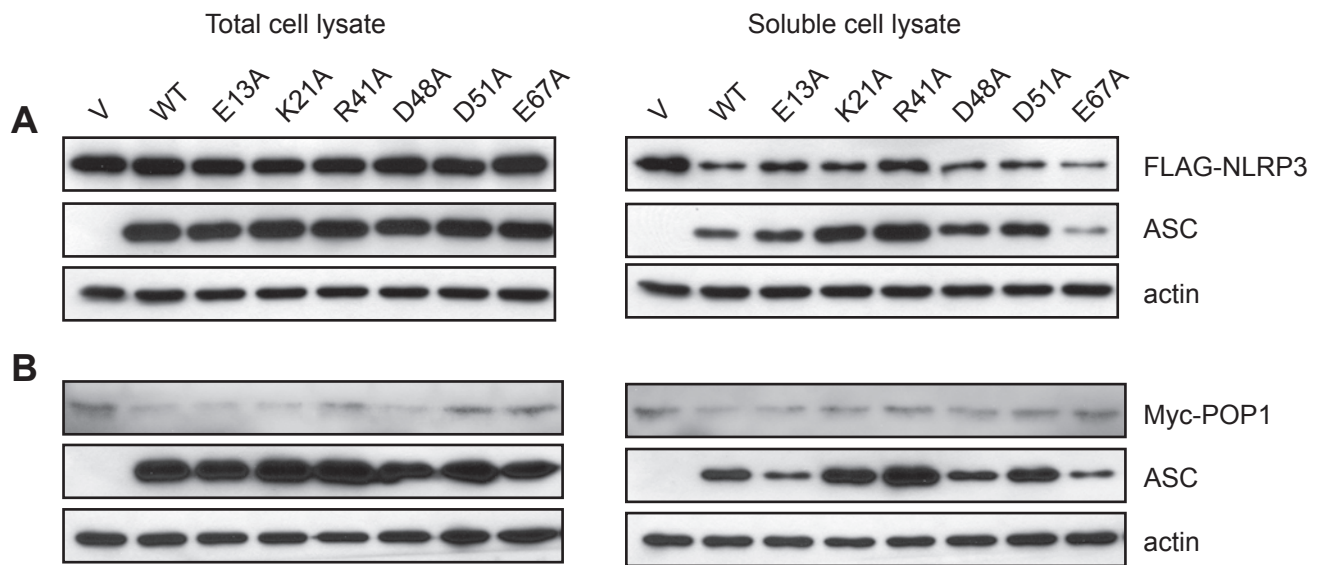
FIGURE S1. Western blot analysis of total cell lysates and soluble cell lysates from cells coexpressing wild-type or mutant ASC and interacting proteins. Plasmids expressing wild-type or mutant ASC, or empty vector (V) were co-transfected with plasmids expressing either **(A)** FLAG-tagged NLRP3 or **(B)** Myc-tagged POP1 in HEK 293T cells. Cells were lysed with lysis buffer and centrifuged at 14 000 g to remove cell debris and insoluble proteins. Aliquots of total cell lysate (taken prior to centrifugation) and the soluble cell lysate (taken from the supernatant after centrifugation) were analysed by western blotting. The level of β-actin was used as an internal loading control and was detected using an anti-β-actin antibody.
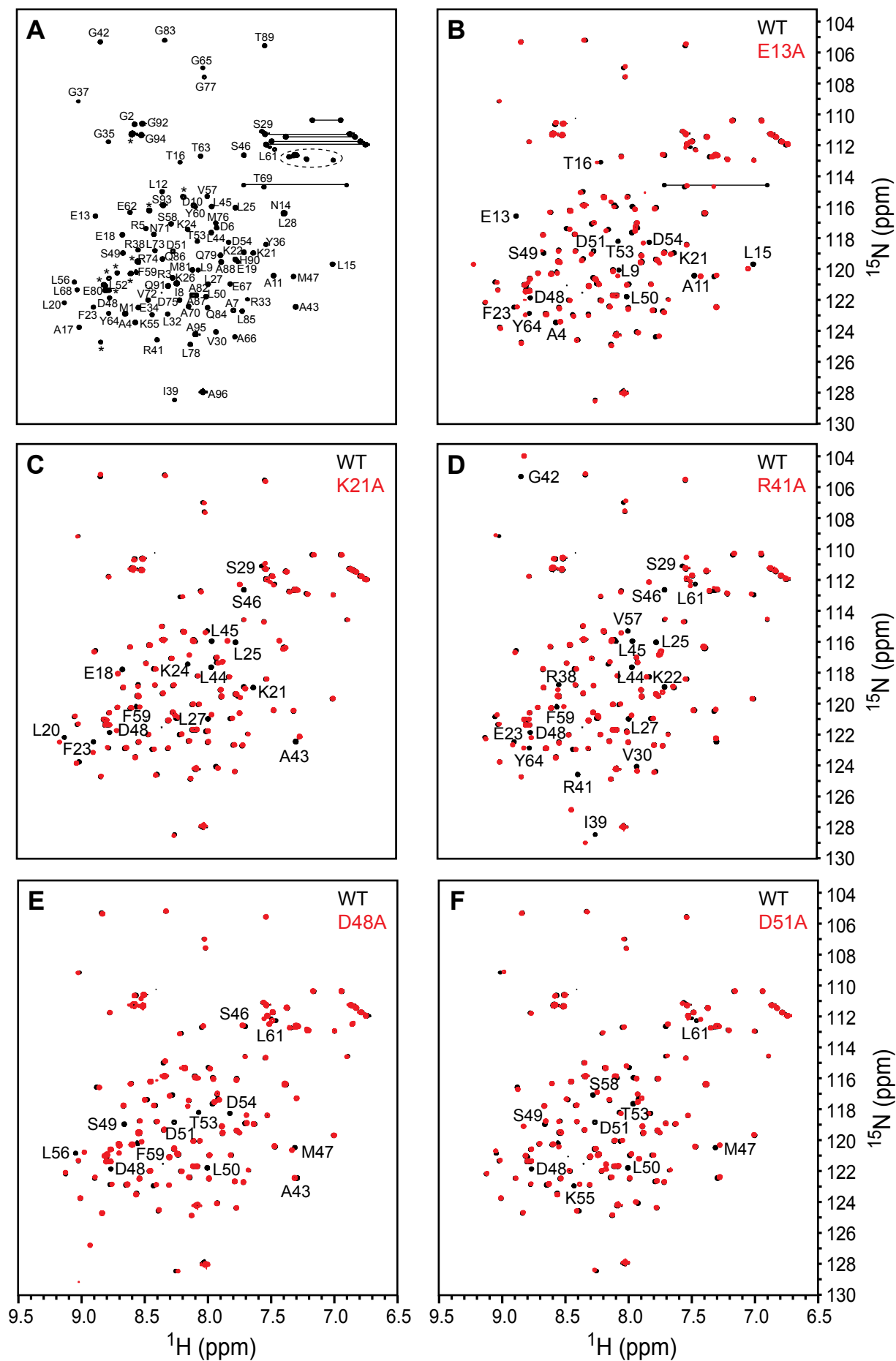
FIGURE S2. The key binding-defective ASC PYD mutants retain structural integrity. (A) 2D ^{1}H-^{15}N HSQC spectrum and backbone resonance assignments of wild-type ASC PYD. The spectrum was recorded in 50 mM sodium phosphate pH 4 and 150 mM NaCl at 25°C. Assignments of residues are indicated with the one-letter amino acid code and the sequence number. Horizontal lines connect peaks corresponding to side chain NH$_2$ groups of Asn and Gln residues. Residues corresponding to the His$_6$-tag are indicated by asterisks and arginine side chain Nε peaks are circled. **(B-F)** Overlay of the 2D ^{1}H-^{15}N HSQC spectra of wild-type (black) and mutant (red) ASC PYD proteins E13A, K21A, R41A, D48A and D51A, respectively.

FIGURE S3. Assessment of structural integrity of ASC PYD mutants that disrupted interaction with POP1 only. (A-D) Overlay of the 2D ^{1}H-^{15}N HSQC spectra of wild-type (black) and mutant (red) ASC PYD proteins R3A, D10A, R38A and D54A, respectively.

α1   α2   α3

human   MGR-ARDAILDAL**E**NLTAEEL**K**KFKLKLLSVPLREGYGRIP**R**GALLSM-**D** 48
monkey   MGR-ARDAILDAL**E**NLTAEEL**K**KFKLKLLSVPLREGYGRIP**R**GALLSM-**D** 48
elephant   MWR-ARDAILEAL**E**YLTADEL**R**RFKMKLLSVQLRDGYGRIP**R**GSLLPM-**D** 48
dog   MGR-IRDAILDAL**E**NLTAEEF**K**KFKMKLLSVPLREGYGRIP**R**GTLLPM-**D** 48
horse   MGR-TRDAILEAL**E**NLTADEL**K**KFKMKLLSVPLREGYGRIP**R**GTLLTM-**D** 48
cow   MGC-TRDAILDAL**E**NLTADEL**K**KFKMKLLSVPLREGYGRIP**R**GTLLPL-**D** 48
pig   MGC-TRDAILDAL**E**NLTADEL**K**KFKMKLLSVPLREGYGRIP**R**GTLLPL-**D** 48
mouse   MGR-ARDAILDAL**E**NLSGDEL**K**KFKMKLLTVQLREGYGRIP**R**GALLQM-**D** 48
rat   MGR-ARDAILDAL**E**NLTADEF**K**KFKMKLLTAPVREGYGRIP**R**GALLQM-**D** 48
chinese hamster MG---RDAILDAL**E**NLTADEL**K**KFKMKLLSVPLREGYGRIP**R**GTLLPM-**D** 46

frog   MGQTVRDLLLETL**E**ELGEKQF**K**KFKGKLNDWEVNAGYKVIP**K**CRLEKA-**D** 50

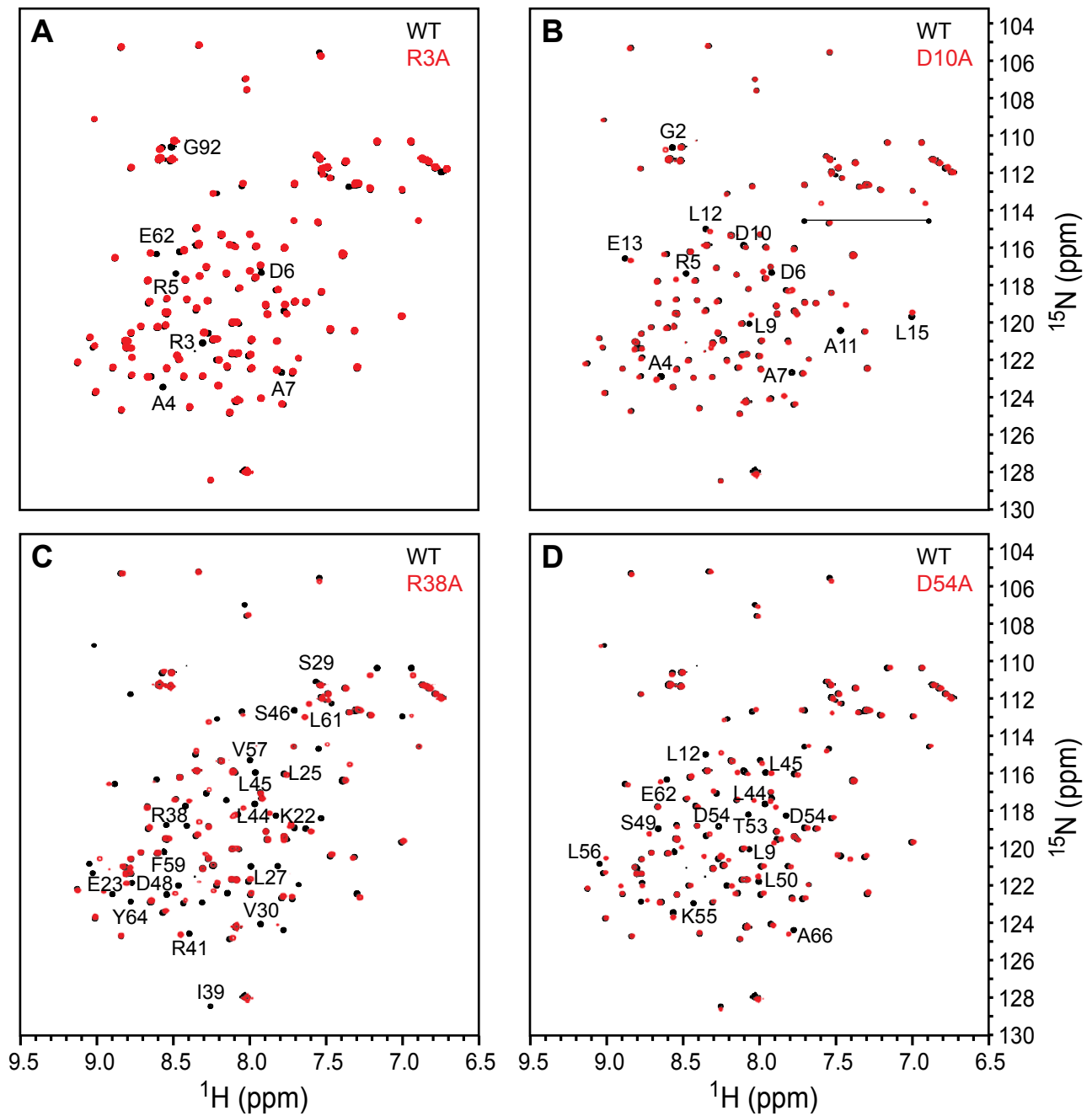rainbow trout   MSKTVGDILIGVL**D**DLGEAEL**K**KFRRKLCDRK---QEPKVR**R**GIVEKA-**D** 47
zebrafish   MAESFKEHLQEAF**E**DLGADNL**R**KFKSKLGDRR---QEPRVT**K**SAIEKLK**D** 48
salmon   MSKTVGDILIGVL**D**DLGEAEL**K**KFRRKLCDRK---QEPKVR**R**GIVEKA-**D** 47

α4   α5   α6

human   AL**D**LTDKLVSFYLETYGAELTANVLRDMGLQEMAGQLQAATHQGSGAAPAG 99
monkey   AL**D**LTDKLVSFYLEAYGAELTANVLRDMGLHETAGQLQAATHQGSGAAPAG 99
elephant   AV**D**LTDKIVSFYLEEYGAELTAVVLREIGMRETAEQLQMQIN--------- 90
dog   AM**D**LTDKLVSFYLEEYGAELTAVVLRDIGMQETAERLQETSHKGHTPGPAG 99
horse   AM**D**LTDKLVSFYLEAYGAELTELVLRDMGMQETAERLQEITRK------- 91
cow   AV**D**LTDKLVSYYLEAYGAELTALVLRDMGMQEVAEQLQETMSKGPRNVLAE 99
pig   AI**D**LTDKLVNYYLEEYSAELTALVLRDIGMKEVAEQLQKTLHKGPGAKPAG 99
mouse   AI**D**LTDKLVSYYLESYGLELTMTVLRDMGLQELAEQLQTTKE-ESGAVAAA 98
rat   PI**D**LTDKLVSYYLEGYGLELTMSVLRDMGIQELAEQLQKIME-ESGAVATA 98
chinese hamster AM**D**LTDKLVSFYLEAYGMELTMTVLREMGMQELAEQLQMVIQKESKAVATA 97

frog   ED**D**VADLIISFYAETYGIEVTLGVLEAIGEMKHHGKLRKSWQEVAAPTPSV 100

rainbow trout   PV**D**LVDILTRTFTEDGAVNVAIEVLAAINCQDVAKELMEFKKSPGSCVTSG 97
zebrafish   EI**D**LADLMVGVFTSKDAVSVTVEILRAIKCIAVADDLLRNTGQSESKGAPS 98
salmon   PV**D**LVDILTRTFTEDGAVNVAIEVLGAINCQDVAEELTEFK---KSQGSCV 94
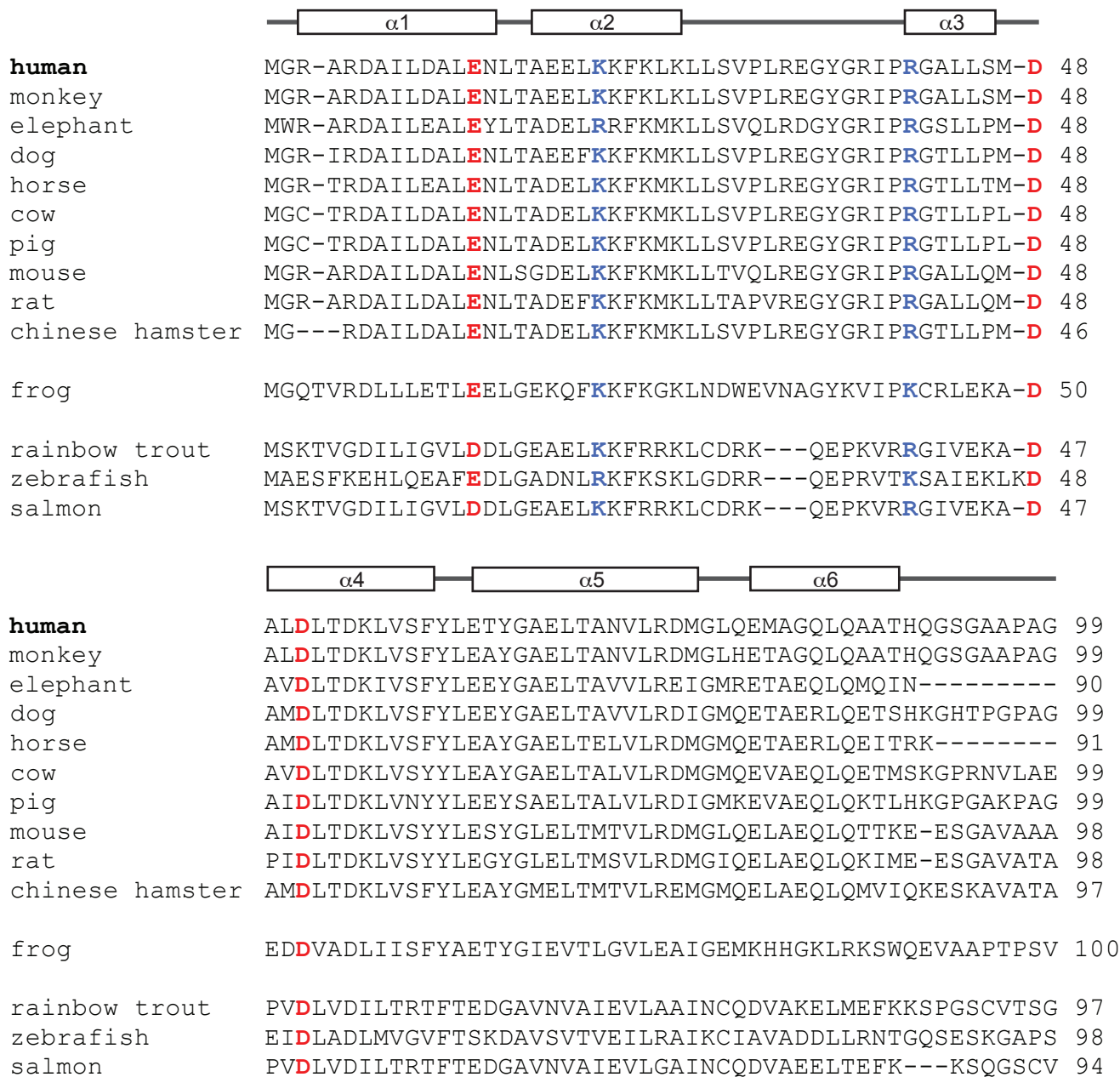
FIGURE S4. The key residues important for ASC interactions are conserved across diverse species. Sequence alignment of ASC sequences with accession numbers BAA87339.2 (human), NP_001181501.1 (monkey), XP_003418917.1 (elephant), XP_003639139.1 (dog), XP_001500559.1 (horse), NP_777155.1 (cow), XP_003124516.1 (pig), NP_075747.3 (mouse), NP_758825.1 (rat), EGW03251.1 (chinese hamster), NP_001086388.1 (frog), ACO08655.1 (rainbow trout), NP_571570.2 (zebrafish), ACN12209.1 (salmon). The conserved acidic and basic residues that mediate ASC PYD interactions are coloured red and blue, respectively.
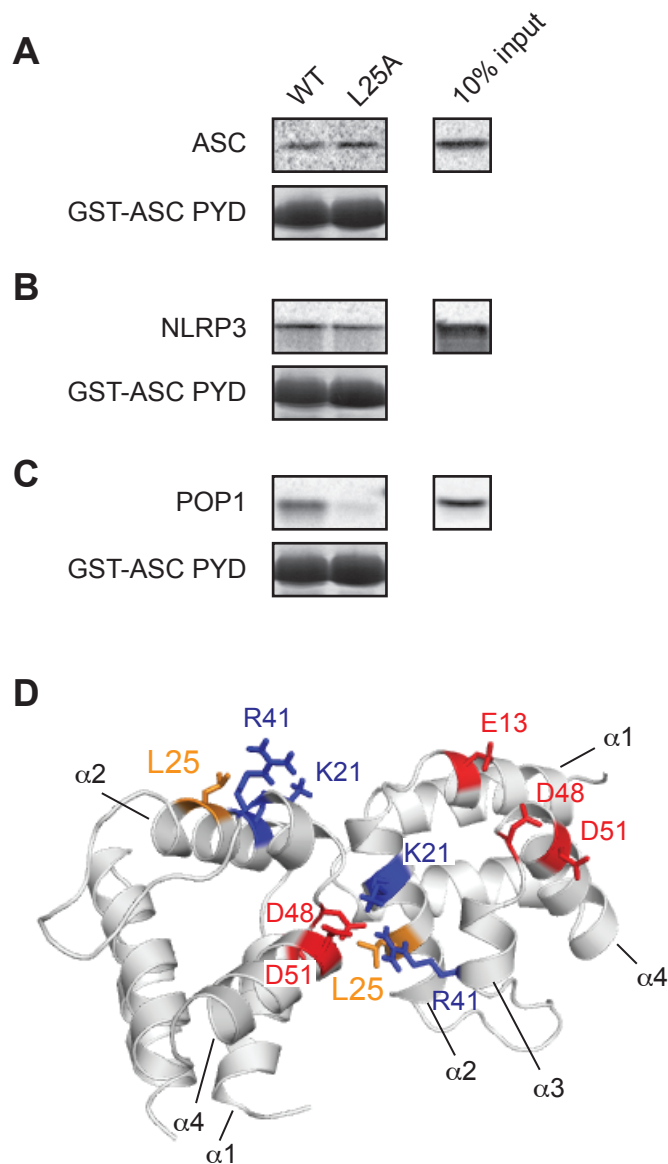
FIGURE S5. The L25A mutation in ASC PYD disrupts interaction with POP1 but not self-association or interaction with NLRP3. Purified bead-bound wild-type or L25A mutant GST-ASC PYD was used in binding assays with in vitro translated 35S-methionine-labelled **(A)** ASC, **(B)** NLRP3 or **(C)** POP1. Bound protein was eluted with SDS-PAGE sample buffer and subjected to SDS-PAGE. GST-ASC PYD was detected by Coomassie stain, while 35S-labelled proteins were detected by phosphorimaging. An amount representing 10% of the input used for binding studies is shown. **(D)** Ribbon representation of the ASC PYD homodimer model with the residues important for binding shown in red (acidic residues) and in blue (basic residues), and L25 is shown in orange.
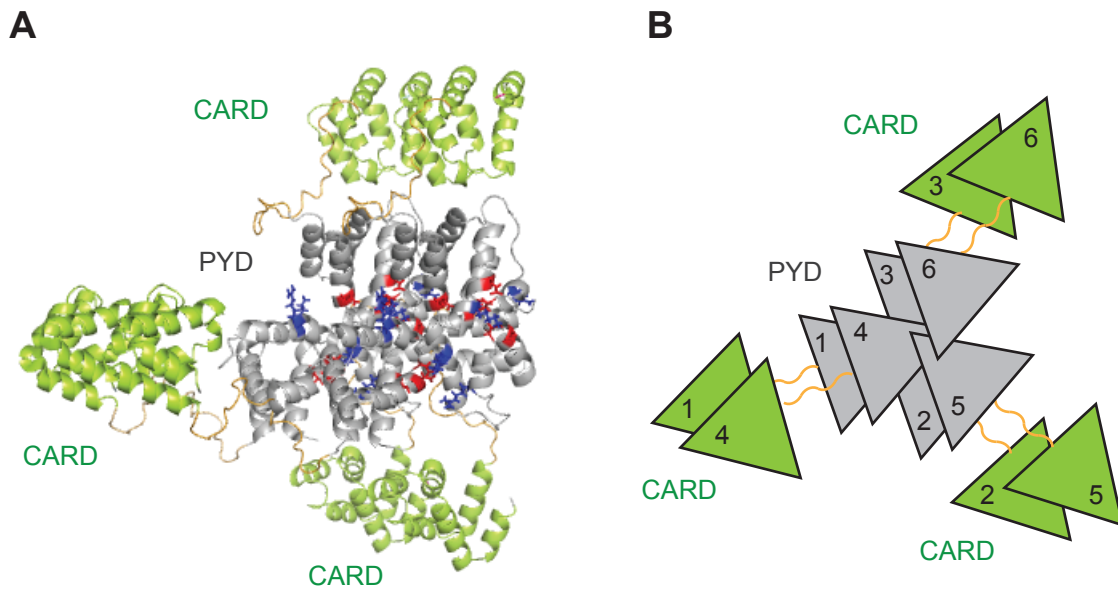
FIGURE S6. Assembly of full-length ASC into a higher order oligomer. (A) The PYDs of the ASC PYD hexamer (Figure 9) were superimposed with the PYDs of full-length ASC. **(B)** Schematic of the full-length ASC hexamer. In both (A) and (B), PYDs are shown in grey, CARDs are shown in green, and the linker is shown in orange.
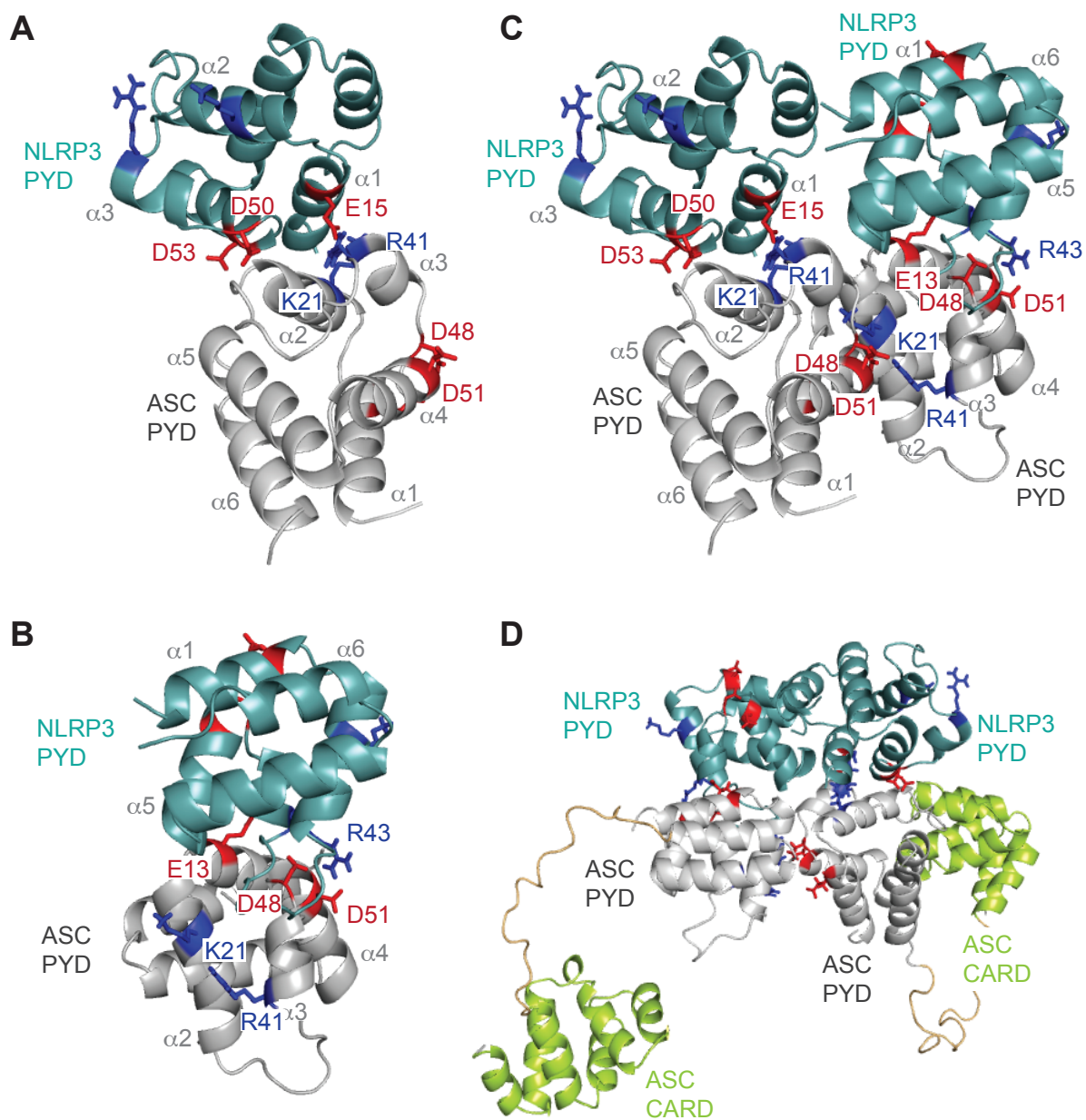
FIGURE S7. Putative models of the NLRP3/ASC PYD complex. Putative models of ASC/NLRP3 PYD heterodimers were generated using HADDOCK. The NLRP3 PYD (PDB ID code 3QF2) (39) and ASC PYD (PDB ID code 1UCP) (37) were used as starting structures for the docking calculations. **(A)** For one ASC/NLRP3 PYD heterodimer, K21 and R41 were defined as active residues for ASC PYD, while E15, D50 and D53 were defined as active residues for NLRP3 PYD. **(B)** For the second heterodimer, E13, D48 and D51 were defined as active residues for ASC PYD, while K23 and R43 were defined as active residues for NLRP3 PYD. **(C)** To demonstrate how ASC PYD can simultaneously self-associate and interact with NLRP3, the ASC PYDs of the two ASC/NLRP3 PYD heterodimers were aligned with ASC PYDs of the homodimer. **(D)** As in (C), except that ASC PYDs were replaced with full-length ASC by superimposing the PYDs of full-length ASC with the PYDs of the homodimer. In all panels, NLRP3 PYD is shown in blue while ASC PYD is shown in grey, and in (D), ASC CARD is shown in green and ASC linker is shown in orange.

A


```
                    α1              α2                      α3
ASC       -----MGRARDAILDALENLTAEELKKFKLKLLSVPLREGYGRIPRGALLSMD  48
POP1      -----MGTKREAILKVLENLTPEELKKFKMKLGTVPLREGFERIPRGALGQLD  48
NLRP3     MKMASTR---CKLARYLEDLEDVDLKKFKMHLEDYPPQKGCIPLPRGQTEKAD  50

NLRP1     ----MAGGAWGRLACYLEFLKKEELKEFQLLLANKAHSRSSSGETPAQPEKTS  49
NLRP7     ---MTSPQLEWTLQTLLEQLNEDELKSFKSLLWAFPLEDVLQKTPWSEVEEAD  50
NLRP10    MAMAKARKPREALLWALSDLEENDFKKLKFYLRDMTLSEGQPPLARGELEGLI  53
mNLRP10   MALARANSPQEALLWALNDLEENSFKTLKFHLRDVT----QFHLARGELESLS  49
NLRP12    MLRTAGRDGLCRLSTYLEELEAVELKKFKLYLG-TATELGEGKIPWGSMEKAG  52
```

```
                 α4            α5              α6
ASC       ALDLTDKLVSFYLETYGAELTANVLRDMGLQEMAGQLQAAT  89
POP1      IVDLTDKLVASYYEDYAAELVVAVLRDMRMLEEAARLQRAA  89
NLRP3     HVDLATLMIDFNGEEKAWAMAVWIFAAINRRDLYEKAKRDE  91

NLRP1     GMEVASYLVAQYGEQRAWDLALHTWEQMGLRSLCAQAQEGA  90
NLRP7     GKKLAEILVNTSSENWIRNATVNILEEMNLTELCKMAKAEM  91
NLRP10    PVDLAELLISKYGEKEAVKVVLKGLKVMNLLELVDQLSHIC  94
mNLRP10   QVDLASKLISMYGAQEAVRVVSRSLLAMNLMELVDYLNQVC  90
NLRP12    PLEMAQLLITHFGPEEAWRLALSTFERINRKDLWERGQRED  93
```
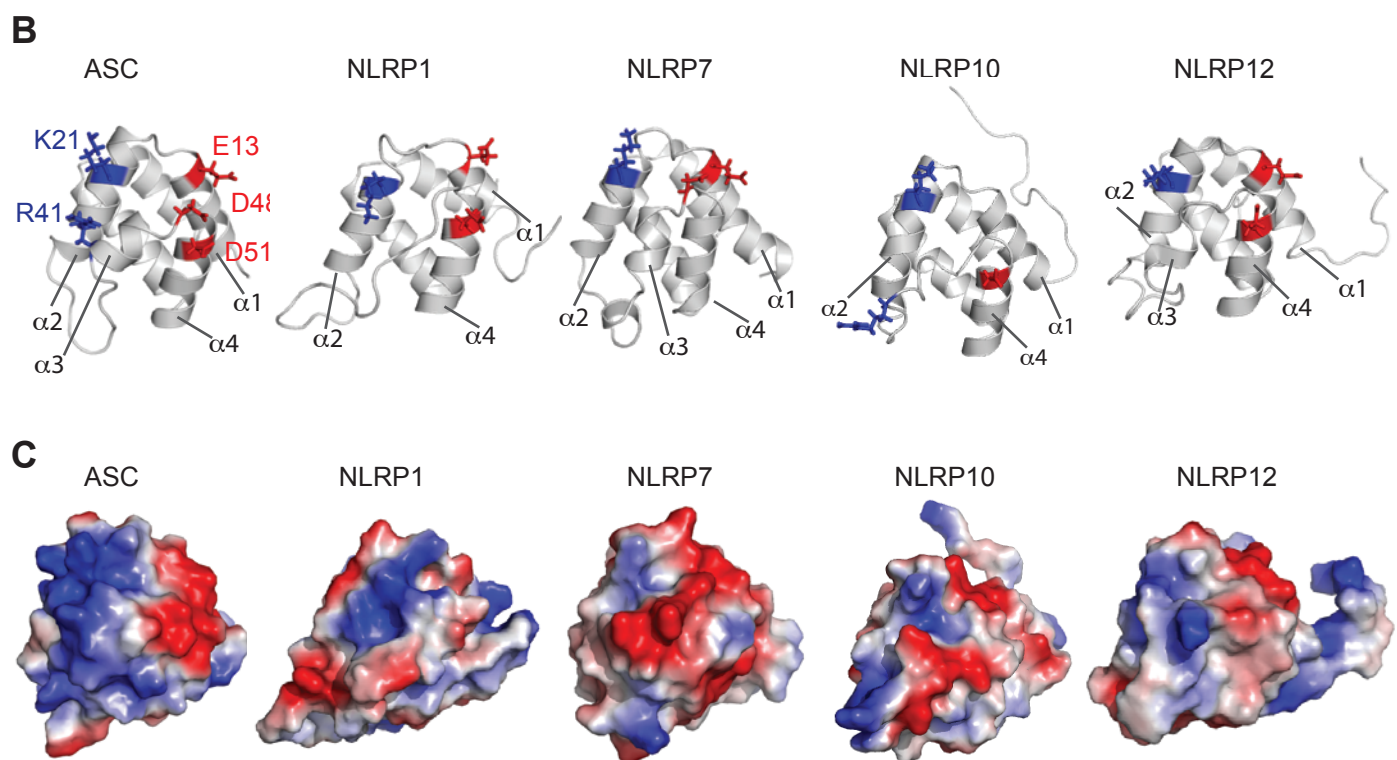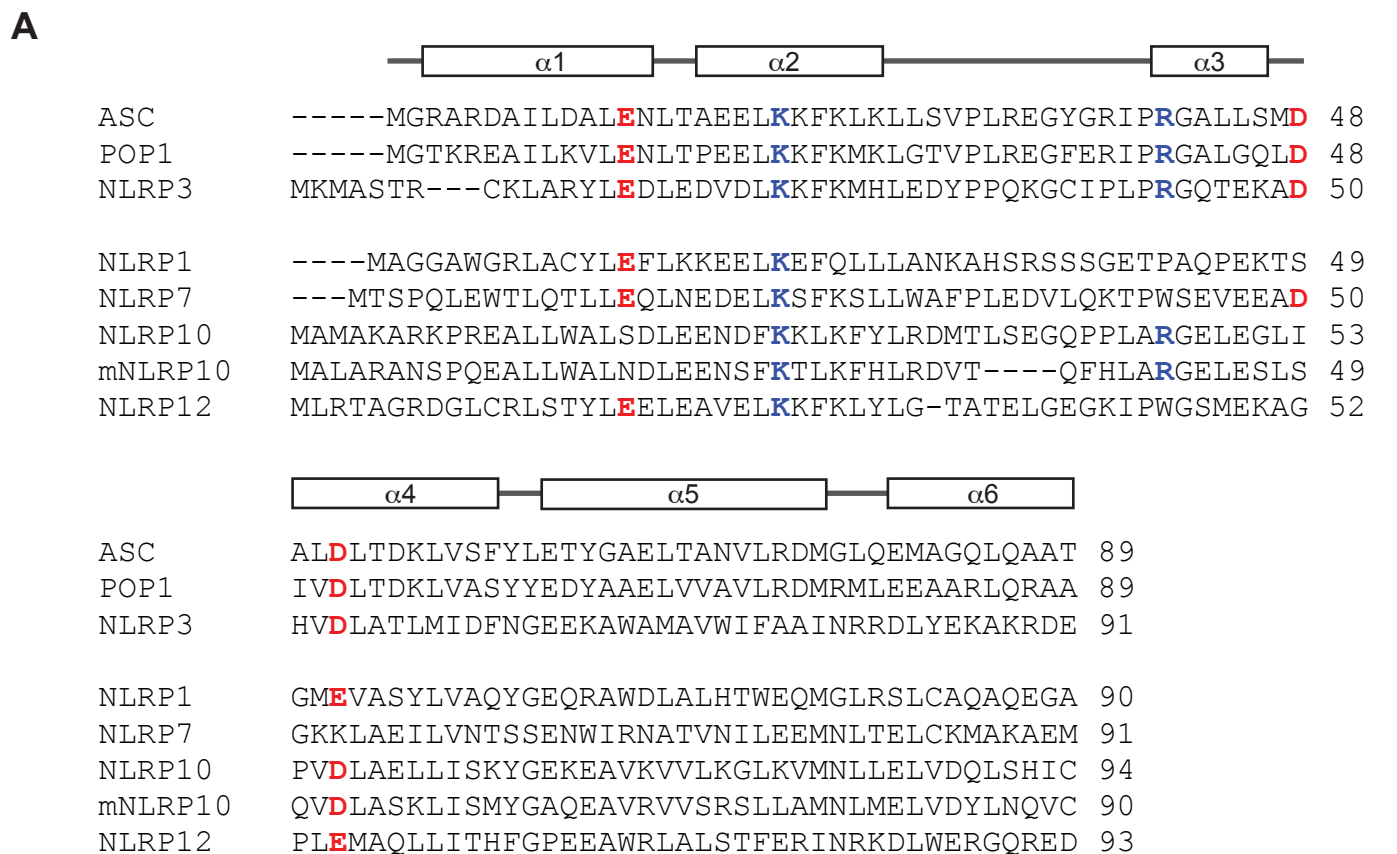
B

C

FIGURE S8. Residues critical for interaction of the ASC PYD are not conserved in NLRP1, NLRP7, NLRP10 and NLRP12. (A) Amino acid sequence alignment of the PYDs of ASC, POP1, NLRP3, NLRP1, NLRP7, NLRP10, murine NLRP10 and NLRP12. Acidic and basic residues important for all interactions of the ASC PYD are coloured red and blue, respectively. (B) Structures of the PYDs from ASC (PDB ID code 1UCP) (37), NLRP1 (PDB ID code 1PN5) (38), NLRP7 (PDB ID code 2KM6) (40), murine NLRP10 (PDB ID code 2DO9) and NLRP12 (PDB ID code 2L6A) (41) were aligned using PyMol and the residues important for interaction of the ASC PYD are indicated with acidic residues in red and basic residues in blue. (C) Surface electrostatic potential of the PYDs of ASC, NLRP1, NLRP7, NLRP10, and NLRP12. Surface views are shown in the same orientation as panel (B).

Multiple Binding Sites on the Pyrin Domain of ASC Protein Allow Self-association and Interaction with NLRP3 Protein

Parimala R. Vajjhala, Ruth E. Mirams and Justine M. Hill

Access the most updated version of this article at doi: 10.1074/jbc.M112.381228

Alerts:
- When this article is cited
- When a correction for this article is posted

Click here to choose from all of JBC's e-mail alerts

Supplemental material:
http://www.jbc.org/content/suppl/2012/10/12/M112.381228.DC1.html

This article cites 63 references, 19 of which can be accessed free at
http://www.jbc.org/content/287/50/41732.full.html#ref-list-1